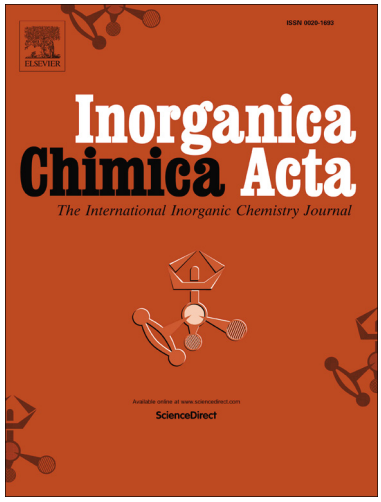

Research paper

Pyridine aided progression from amorphous to crystalline bis([5-(aryl)-1-diazenyl]quinolin-8-olato)zinc(II) compounds – Solution and solid-state structural characterization, nanoparticle formation and antibacterial activity

Tushar S. Basu Baul, Khrawborlang Nongsiej, Koel Biswas, Santa Ram Joshi, Herbert Höpfl

PII: S0020-1693(18)30501-2
DOI: https://doi.org/10.1016/j.ica.2018.06.049
Reference: ICA 18341

To appear in: *Inorganica Chimica Acta*

Received Date: 4 April 2018
Revised Date: 28 June 2018
Accepted Date: 28 June 2018

Please cite this article as: T.S. Basu Baul, K. Nongsiej, K. Biswas, S.R. Joshi, H. Höpfl, Pyridine aided progression from amorphous to crystalline bis([5-(aryl)-1-diazenyl]quinolin-8-olato)zinc(II) compounds – Solution and solid-state structural characterization, nanoparticle formation and antibacterial activity, *Inorganica Chimica Acta* (2018), doi: https://doi.org/10.1016/j.ica.2018.06.049

Pyridine aided progression from amorphous to crystalline bis([5-(aryl)-1-diazenyl]quinolin-8-olato)zinc(II) compounds – Solution and solid-state structural characterization, nanoparticle formation and antibacterial activity

Tushar S. Basu Baul,[a,*] Khrawborlang Nongsiej,[a] Koel Biswas,[b] Santa Ram Joshi[b] and Herbert Höpfl[c,*]

[a]*Centre for Advanced Studies in Chemistry, North-Eastern Hill University, NEHU Permanent Campus, Umshing, Shillong 793 022, India*

[b]*Department of Biotechnology & Bioinformatics, North-Eastern Hill University, NEHU Permanent Campus, Umshing, Shillong 793 022, India*

[c]*Centro de Investigaciones Químicas, Instituto de Investigación en Ciencias Básicas y Aplicadas, Universidad Autónoma del Estado de Morelos, Av. Universidad 1001, Cuernavaca 62209, Mexico*

Abstract

Ten new zinc(II) compounds, viz. $[Zn(L^{Q})_2(4\text{-}MePy)_2]\cdot H_2O$ (**1**), $[Zn(L^{MeAQ})_2(Py)_2]\cdot C_6H_6$ (**2a**), $[Zn(L^{MeAQ})_2(H_2O)_2]$ (**2b**), $[Zn(L^{OMeAQ})_2(H_2O)_2]$ (**3**), $[Zn(L^{EtAQ})_2(3\text{-}MePy)_2]$ (**4**), $[Zn(L^{OEtAQ})_2(4\text{-}MePy)_2]\cdot 0.5C_6H_7N$ (**5a**), $[Zn(L^{OEtAQ})_2(H_2O)_2]$ (**5b**), $[Zn(L^{NMe2AQ})_2(Py)_2]\cdot 1.5C_6H_6\cdot H_2O$ (**6**), $[Zn(L^{CAQ})_2(Py)]$ (**7**) and $[Zn(L^{BAQ})_2(Py)]$ (**8**) (primary ligands: L^{Q} = quinolin-8-olate and L^{XAQ} = 4-substituted 5-[(*E*)-2-(aryl)-1-diazenyl]quinolin-8-olate; secondary ligands: Py = pyridine, 3-MePy = 3-methylpyridine, 4-MePy = 4-methylpyridine) have been synthesized and characterized by elemental analysis, IR, NMR, UV-vis and fluorescence spectroscopy and single-crystal X-ray diffraction analysis. The structural characterization revealed a distorted octahedral geometries for **1**-**6**, in which *trans*-disposed 8-quinolate ligands occupy the equatorial and the secondary ligands the axial positions. Compounds **7**-**8** comprise five-coordinate molecular structure with square-pyramidal coordination polyhedra based on *trans*-oriented quinolate ligands and a Py molecule in the apical position. In the crystal structures of **1**-**8**, the molecules are assembled by π–stacking interactions and for the aquo-compounds additionally by O–H···O hydrogen bonds. As representative example, compound **2a** was used as starting material for the synthesis of ZnO nanoparticles in an average size range of 70–120 nm, as illustrated by PXRD analysis and TEM images. The antimicrobial activity of the pro-ligands and zinc(II) compounds studied herein was assessed by inhibition zone test in agar cultures against five indicator bacterial strains, i.e. *Escherichia coli* MTCC 730, *Streptococcus pyogenes* MTCC 1925, *Klebsiella pneumoniae* MTCC 109, *Bacillus cereus* MTCC 430 and *Salmonella enterica* MTCC 735.

Keywords: substituted quinolin-8-olate, zinc, secondary ligands, structure elucidation, nanoparticles, antimicrobial activity

---

* Corresponding authors. *E-mail addresses*: basubaulchem@gmail.com; basubaul@nehu.ac.in (T. S. Basu Baul), hhopfl@uaem.mx (Herbert Höpfl)

1. Introduction

Quinolin-8-ol (HL^Q), a well-known bidentate chelating ligand, has been utilized for the qualitative and quantitative analysis of metal ions in gravimetric analysis to selectively bind and precipitate metal ions [1,2]. In addition, quinolin-8-olate metal compounds are extensively used in areas such as photochemical processes [3-7] and optical sensing [8-10]. The high thermal stability, excellent electron transport properties and the unique electroluminescent properties of tris(quinoline-8-olato)aluminium (III) [$Al(L^Q)_3$] provided a pivotal role in the development of organic light-emitting diodes (OLEDs) that lead to the introduction of the flat-panel display technology [11]. This innovation has stimulated research groups' world wide to develop further compounds based on derivatives of HL^Q including derivatives with other metal ions. Of special interest is the tuning of the emission color of metal-based OLEDs, which is achieved via the introduction of substituents in the 2-, 4-, 5- and 7-position of the HL^Q ligand [12]. A more recent approach is based on modifications of the supramolecular interaction patterns of HL^Q compounds [13].

In addition, HL^Q has emerged as a privileged scaffold for the development of new drug candidates, such as fungicidal, insecticidal, anti-microbial, anti-oxidant, anti-inflammatory, anti-neurodegenerative and antitumor/antineoplastic agents [14-25]. In bacteria, zinc performs a beneficial role in enzymatic processes and the organization of protein structures [26]. Nevertheless, at high concentrations an inhibitory action on the growth of bacterial species such as *Escherichia coli*, *Staphylococcus aureus*, *Staphylococcus faecalis*, *Staphylococcus epidermidis* and *Proteus aeruginosa* is observed [27,28]. It is also known that the interaction of zinc with bioactive organic compounds can increase the biological activity [29], while other metals inhibit their activity [30]. In this context, clioquinol (5-chloro-7-iodoquinolin-8-ol), which is an antimicrobial agent known for many years [31] has been combined with a series of 3d metal compounds, showing that the antimicrobial activities vary depending on the microorganism and metal used for complex formation [32].

Zinc(II) cations can adopt various coordination geometries, giving a versatile complexation chemistry with HL^Q (Chart 1). Usually 2:1 complexes are obtained, but 3:1 complexes can also be formed [33]. The preparation of bis(quinolin-8-olato)zinc(II), [$Zn(L^Q)_2$], if carried out in aqueous medium, the corresponding diaquo compound is formed, i.e. [$Zn(L^Q)_2(H_2O)_2$], in which two water molecules are bound in *trans*-fashion to the square-planar

$Zn(L^Q)_2$ moiety (**I**) [34]. With the 5-nitro-HL^Q analog a related structure was reported, but in this case the compound crystallized as methanol solvate [35]. Anhydrous zinc(II) quinolin-8-olate consists of four 2:1 complex units linked to a linear tetramer, $[Zn(L^Q)_2]_4$ (**II**), in which the zinc atoms are connected by bridging quinolin-8-olate oxygen atoms [36]. Similar to $[Al(L^Q)_3]$, $[Zn(L^Q)_2]$ was explored for the fabrication of electroluminescent devices, showing good electron-transport properties due to π-stacking interactions of the metal-coordinated ligands within the crystal structure [36,37]. Both dimeric $[Zn(L^Q)_2]_2$ (**III**) and trimeric $[Zn(L^Q)_2]_3$ (**IV**) compounds are formed when the quinolin-8-olate ligands are substituted in the 7- or 2-position [38,39]. In trimeric (**IV**), the cyano-substitution induces strong red-light emission [39]. On the other hand, lipophilic quinolin-8-ol derivatives featuring substitution at the 2- as well as in the 7-position by methyl and long alkyl groups revealed compounds of composition $[Zn(L^Q)_2]$ (**V**) with a pseudo-tetrahedral coordination geometry at the zinc(II) center, possibly as a consequence of the steric bulk [38a]. The supramolecular solid-state assembly can be also modified by introduction of an amide substituent into the quinolin-8-olate ring, featuring a polymeric network, $[Zn(L^Q)_2(\mu\text{-}Q)]_n$ (**VI**), with penta-coordinated distorted square-pyramidal zinc centers through the formation of C=O→Zn bonds via the amide oxygen atoms [40]. In the presence of strong metal-coordinating solvents, the product obtained from equimolar reactions of ZnX_2 (X = Cl or Br) with HL^Q in methanol, e.g. dimethylformamide, dimethylacetamide and dimethysulphoxide, afforded the respective solvate of a tetranuclear cluster of composition $[Zn_4(L^Q)_6X_2]\cdot 2$ solvent (**VII**). Using the sterically more hindered 3-methylpyridine ligand, a compound containing mononuclear zinc ions resulted, $[Zn(L^Q)_2(3\text{-MePy})]\cdot[Zn(L^Q)_2(3\text{-MePy})_2]\cdot 3H_2O$ (**IX**) [41]. In **VII**, the $[Zn_4(L^Q)_6X_2]$ core displays two different coordination environments for the zinc cations. The zinc sites holding the halide ions are penta-coordinated, while the remaining zinc sites are hexa-coordinated giving a distorted octahedral coordination polyhedron. On the other hand, the zinc atoms in the molecular compounds portrayed in **IX** adopt a five-coordinate distorted square-pyramidal and a distorted octahedral geometry, in which the 3-methylpyridine molecules occupies the apical and axial positions, respectively. Reaction of zinc chloride with HL^Q in an equimolar ratio followed by crystallization from water afforded the tetrachlorozincate salt of $[HQH]^+$, i.e. $(H_2L^Q)_2[ZnCl_4]$ (**VIII**) (H_2L^Q is quinolin-1-ium-8-ol) [42,43].

The luminescent properties of HL^Q ligands can be tailored by extending the π-electron system with additional functional groups [44]. In line with this strategy, several zinc(II)

compounds have been reported. [(2,6-Dichlorophenyl)ethenyl]quinolin-8-olate), here after L^{SQ}, gave a complex of composition $[Zn_2(L^{SQ})_2]_2$ and the structure reveals the same binuclear core and a trigonal-bipyramidal geometries around Zn atoms as shown in Chart 1 (**III**) [38b]. In contrast to $[Zn(L^{SQ})_2]_2$, with [(2,6-difluorophenyl)-, [(2,4-dinitrophenyl)- [44a] and [(2,4,6-trifluorophenyl)ethenyl]quinolin-8-olates [44c] unique trimeric zinc(II) compound of formulation $[Zn(L^{SQ})_2]_3$ (**X**) were obtained. The SCXRD analyses indicated that the terminal zinc atoms in the trimeric unit have distorted trigonal-bipyramidal geometries with the equatorial plane occupied by the N_2O donor atoms of three different ligands and the apical positions formed by the phenoxy oxygen atoms of two ligand molecules. On the contrary, the coordination environment of the central Zn(II) atom is a distorted octahedron, where the equatorial plane is occupied by the NO_3 donors from three ligands, while the apical positions are occupied by one phenoxy oxygen atom and a quinoline nitrogen atom. Because of the promising properties and potential applications of luminescent coordination polymers, in a subsequent development of this ligand type, 3- and 4-pyridyl-substituted quinolin-8-olates were explored, giving 1D coordination polymers of the type $\{[Zn(L^{3\text{-}SQ})(X)]_2\}_n$ (**XI**) ($L^{3\text{-}SQ}$ = [(3-pyridyl)ethenyl]quinolin-8-olate, X = Cl, Br or I) [44e] and $\{[Zn(L^{3\text{-}SQ})_2(\mu\text{-}L^{3\text{-}SQ})_2]\}_n$ (**XII**). In **XI**, the basic building unit comprises a dinuclear Zn compound, in which two-phenolate oxygen atoms of two ligands bridge the metal atoms. The five-coordinate Zn(II) centers are bound to the quinoline and pyridyl nitrogen atoms from two ligands L, two phenolate oxygen atoms and one halide anion, establishing a distorted trigonal-bipyramidal geometry [44e]. In **XII**, the building blocks are mononuclear with the Zn(II) centers adopting a slightly distorted octahedral geometry, in which the equatorial plane is occupied by two chelating NO donor sets from two ligands and the axial positions are constituted by two bridging 4-pyridyl nitrogen atoms of two adjacent ligands [44h]. In summary, quinolin-8-olate-derived ligands have shown to function in a myriad of coordination modes, leading to a large variation of the structural motifs with different coordination numbers and geometries of the zinc(II) atoms (**I**-**XII**, Chart 1).

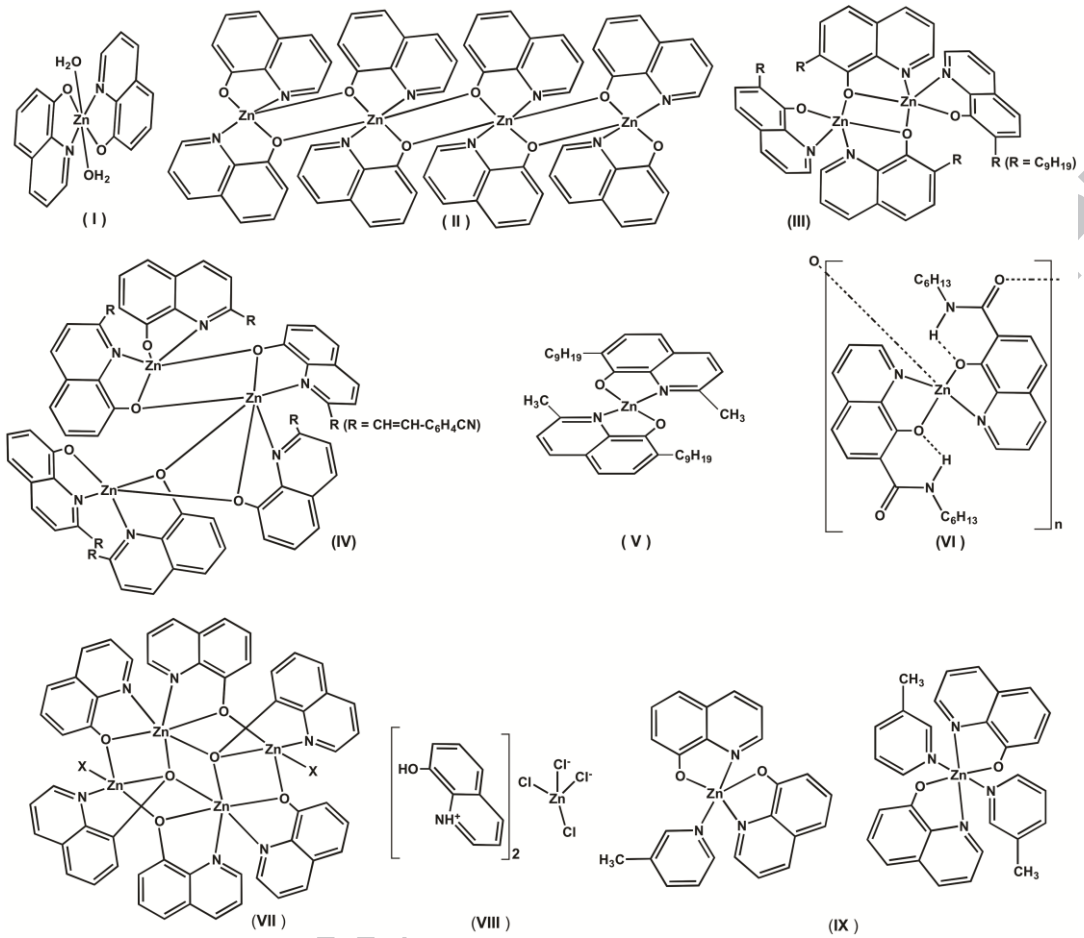

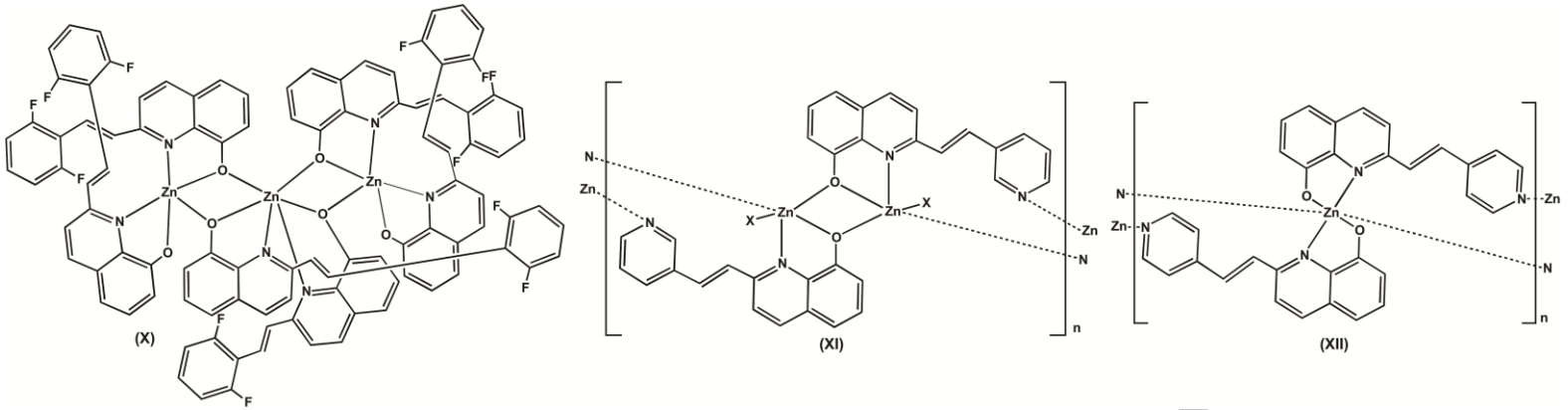

Chart 1. Overview showing the coordination behavior of quinolin-8-olate ligand derivatives towards zinc(II) atoms.

Besides the complexation and structural aspects of zinc(II) quinolin-8-olates, the zinc analog of $[Al(L^{Q})_3]$, i.e. $[Zn(L^{Q})_2]$, has received attention because of its potential to enhance the electron-transporting properties in OLEDs [35,45]. Consequently, the photophysical properties of mono- and multinuclear zinc(II) compounds derived from quinolin-8-olates (Chart 1) are generally analyzed in terms of their molecular structures and the supramolecular solid-state packing [38b,44a,44c,44e,44h]. However, the above-mentioned compounds exhibit divergent photophysical properties and, hence, a conclusive analysis to achieve the tuning of the optical properties has yet not been reached so far. In addition, octahedral $[Zn(L^{Q})_2(H_2O)_2]$ was investigated for photolysis reactions in non-aqueous solvents, revealing that the photo-activation of the water ligand coordinated to zinc(II) is based on the charge shift induced by IL excitation of the quinolin-8-olate ligand. This phenomenon is also found in thermal hydrolysis reactions catalyzed by zinc enzymes in nature [46]. In 1965, Takamoto et al. synthesized a series of 5-(aryl)-1-diazenyl]quinolin-8-ols (HL^{XAQ}) and studied the reactivity in homogeneous media and biphasic systems [47]. Later, the ligands were explored as analytical reagents for the qualitative detection of metal ions [48] and successfully employed for the synthesis of organometallic compounds [49]. More recently, HL^{XAQ} type ligands were grafted on colloidal silica nanoparticles in order to study the kinetics of the complexation with Ni^{2+} ions [50] and to tune the optical properties of structurally characterized rhenium(I) compounds [51]. The complexation chemistry of transition metal [52,53] and rare earth metal [54] complexes with HL^{XAQ} are also on the record. Concerning Zn(II) compounds, there is a report on compounds with ligands having peripheral 4-(X) groups, i.e. 5-[(4-(X)-phenyl)-1-diazenyl]quinolin-8-ol (X = Et, *n*Bu, CMe_3, H and F), which showed interesting luminescent and electroluminescent properties. Particularly, bis(5-[(4-(dimethylamino)phenyl)-1-diazenyl]quinolin-8-olato)zinc(II) showed substantial luminescent quantum yields at room temperature and was identified as electron transport material, which may find applications in photonic devices [52,53], but surprisingly none of these compounds were characterized by X-ray diffraction methods, possibly due to low solubility.

In recent past, we have been focusing on the rational design of various types of discrete compounds and coordination polymers using (*E*)-*N*-(pyridin-2-ylmethylene)arylamine ligands and d^{10} metal ions (Zn, Cd and Hg) [55]. As part of a program enabling the solid-state structural characterization of Zn(II) compounds derived from pro-ligands quinolin-8-ol (HL^{Q}) and 5-[(4-

(X)-phenyl)-1-diazenyl]quinolin-8-ol (HL^{XAQ}) have been reported and, thus providing a series of ten new compounds $[Zn(L^{Q})_2(4\text{-}MePy)_2]\cdot H_2O$ (**1**), $[Zn(L^{MeAQ})_2(Py)_2]\cdot C_6H_6$ (**2a**), $[Zn(L^{MeAQ})_2(H_2O)_2]$ (**2b**), $[Zn(L^{OMeAQ})_2(H_2O)_2]$ (**3**), $[Zn(L^{EtAQ})_2(3\text{-}MePy)_2]$ (**4**), $[Zn(L^{OEtAQ})_2(4\text{-}MePy)_2]\cdot 0.5C_6H_{7N}$ (**5a**), $[Zn(L^{OEtAQ})_2(H_2O)_2]$ (**5b**), $[Zn(L^{NMe2AQ})_2(Py)_2]\cdot 1.5C_6H_6\cdot H_2O$ (**6**), $[Zn(L^{CAQ})_2(Py)]$ (**7**) and $[Zn(L^{BAQ})_2(Py)]$ (**8**), Scheme 1. The zinc(II) compounds were structurally characterized in solution using ^{1}H and ^{13}C NMR, UV-Vis and photoluminescence spectroscopy. Detailed structural information on the molecular and crystal structures of the Zn(II) compounds **1**-**8** was obtained by single-crystal X-ray crystallographic analysis. The results provided three variants of the Zn(II) coordination environment, i.e. $[Zn(L^{XAQ})_2(Py/3\text{-}MePy/4\text{-}MePy)_2]$, $[Zn(L^{XAQ})_2(H_2O)_2]$ and $[Zn(L^{XAQ})_2(Py)]$. Different pyridine ligands were explored as secondary ligands with the objective to vary the molecular and supramolecular structures, envisioning the modification of electronic features for future solid-state applications. As representative case, compound **2a** was used as starting material for the synthesis of ZnO nanoparticles. In addition, the *in vitro* antibacterial activity of **1**-**8** against five strains of bacteria is reported.

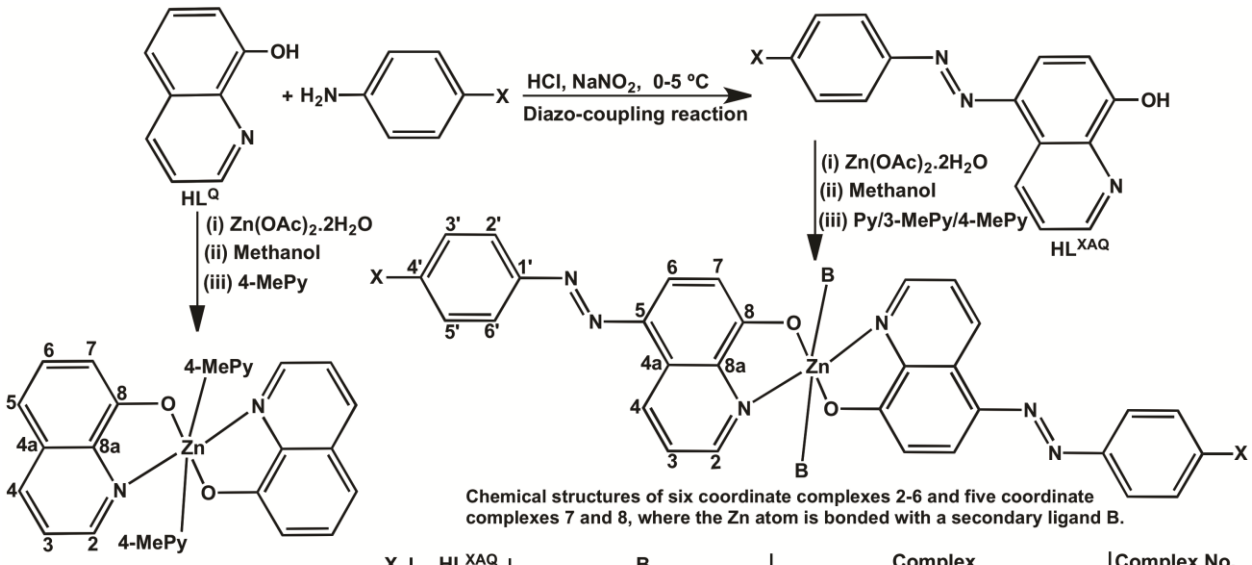

Chemical structures of six coordinate complexes 2-6 and five coordinate complexes 7 and 8, where the Zn atom is bonded with a secondary ligand B.

X	HL^{XAQ}	B	Complex	Complex No.
Me	HL^{MeAQ}	Pyridine (Py)	$[Zn(L^{MeAQ})_2(Py)_2]\cdot C_6H_6$	2a
		Water (H_2O)	$[Zn(L^{MeAQ})_2(H_2O)_2]$	2b
OMe	HL^{OMeAQ}	Water (H_2O)	$[Zn(L^{OMeAQ})_2(H_2O)_2]$	3
Et	HL^{EtAQ}	3-Methylpyridine (3-MePy)	$[Zn(L^{EtAQ})_2(3\text{-}MePy)_2]$	4
OEt	HL^{OEtAQ}	4-Methylpyridine (4-MePy)	$[Zn(L^{OEtAQ})_2(4\text{-}MePy)_2]\cdot 0.5\ (4\text{-}MePy)$	5a
		Water (H_2O)	$[Zn(L^{OEtAQ})_2(H_2O)_2]$	5b
NMe_2	HL^{NMe2AQ}	Pyridine (Py)	$[Zn(L^{NMe2AQ})_2(Py)_2]\cdot 1.5\ (C_6H_6)\cdot H_2O$	6
Cl	HL^{CAQ}	Pyridine (Py)	$[Zn(L^{CAQ})_2(Py)]$	7
Br	HL^{BAQ}	Pyridine (Py)	$[Zn(L^{BAQ})_2(Py)]$	8

Scheme 1. Synthesis of pro-ligand HL^{XAQ} and chemical structures of the zinc(II) complexes **1-8** along with the atom-numbering protocol.

2. Experimental

2.1. General considerations

$Zn(OAc)_2\cdot 2H_2O$ (S.d. fine), 8-hydroxyquinoline (Loba Chemie), *p*-toluidine, *p*-anisidine (CDH), *p*-ethylaniline, *p*-ethoxyaniline, *p*-N,N-dimethylphenyldiamine (Spectrochem), *p*-chloroaniline, *p*-bromoaniline (Himedia), pyridine (Merck), 3-methylpyridine and 4-methylpyridine (Spectrochem) were used without further purification. The solvents used in the reactions were of AR grade and dried using standard procedures.

Melting points were measured using a Büchi melting point apparatus (M-560) and are uncorrected. Carbon, hydrogen and nitrogen analyses were performed with a Perkin-Elmer 2400 series II instrument. IR spectra in the range 4000-400 cm^{-1} were obtained on a Perkin Elmer

Spectrum BX series FT-IR spectrophotometer with samples investigated as KBr discs. ^{1}H and $^{13}C\{^{1}H\}$ NMR spectra, measured at 400.13 and 100.62 MHz, respectively, were recorded on a Bruker AMX 400 spectrometer. The ^{1}H and ^{13}C chemical shifts were referenced to Me_4Si set at δ 0.00 ppm. Absorption measurements were carried out on a Perkin-Elmer Lambda25 spectrophotometer at ambient temperature in freshly prepared DMSO solutions. Emission measurements were carried out on a Hitachi model FL4500 spectrofluorometer with appropriate background correction at ambient temperature in freshly prepared DMSO solutions. Fluorescence spectra in DMSO solutions were obtained with the excitation and emission slits fixed at 10 and 20 nm, respectively, in quartz cuvettes with 10 mm optical path length. Fluorescence quantum yields ϕ_f were determined using acridine yellow in ethanol (ϕ_R = 0.47), based on the following equation:

$$\phi_S = \phi_R \cdot \frac{A_S}{A_R} \cdot \frac{OD_R}{OD_S} \cdot \frac{\eta_S^2}{\eta_R^2}$$

where "A" terms denote the integrated area under the fluorescence curve, "OD" denotes absorbance, η the refractive index of the medium and ϕ, the fluorescence quantum yield. Subscripts "S" and "R" denote the parameters for the studied sample and reference, respectively. Solid-state fluorescence spectra of compound **1** and HL^{Q} were obtained using a Hitachi fluorescence spectrophotometer F-7000 (with the excitation and emission slits fixed at 2.5 and 5 nm, respectively), and spectra were corrected for the instrument response function. For the nanomaterial work, the calcination of **2a** was carried out in a Revotek GMP muffle furnace at a heating rate of 10 °C min^{-1} from 25 °C to 600 °C. Ultrasound irradiations were accomplished with a Sonics VCX 750 instrument equipped with a high intensity ultrasonic probe (13 mm tip diameter; Ti-horn, 20 kHz, 750 Watt) that was immersed directly into the reaction mixture. Powder X-ray diffraction (PXRD) studies were carried out on a GNR X-ray Explorer using Cu*K*α radiation (1.54 Å). For the analysis of the ZnO nanoparticles, a Field Emission Scanning Electron Microscope (FESEM) from Carl Zeiss SIGMA and a Transmission Electron Microscope (TEM), from Jeol (JEM-2100) was used. For the *in vitro* antimicrobial assays, Mueller-Hinton agar (HiMedia) was used as nutrient liquid medium and chloramphenicol (Sigma-Aldrich) as reference antibiotics.

2.2. Synthesis of pro-ligands and zinc(II) compounds

Pro-ligands (HL^{XAQ} viz., HL^{MeAQ}, HL^{OMeAQ}, HL^{OEtAQ}, HL^{CAQ}, HL^{BAQ}) [49a,49b], (HL^{EtAQ} and HL^{NMe2AQ}) [53] were prepared starting from 8-hydroxyquinoline and the corresponding aniline using conventional diazonium salt chemistry, in accordance with literature procedures.

The method employed for the preparations of **1**-**8** are very similar; therefore, only the preparations of $[Zn(L^{Q})_2(4\text{-}MePy)_2]$ (**1**) and $[Zn(L^{MeAQ})_2(Py)_2]\cdot C_6H_6$ (**2a**) are described in detail, as representative examples.

*2.2.1. Synthesis of $[Zn(L^{Q})_2(4\text{-}MePy)_2]\cdot H_2O$ (**1**).* $Zn(OAc)_2\cdot 2H_2O$ (0.23 g, 1.03 mmol) in methanol (10 mL) was added drop-wise to a stirred solution of 8-hydroxyquinoline, HL^{Q} (0.30 g, 2.07 mmol) in methanol (10 mL) at room temperature, which resulted in the immediate formation of straw-colored precipitate. The reaction mixture was heated to reflux for 3 h and then filtered while hot. The residue was washed with hot methanol (3 x 5 mL) to remove undesired materials and dried *in vacuo*. The dried solid was dissolved in hot ethanol (5 mL) containing 4-methylpyridine (1 mL, 10.74 mmol) and filtered while hot. Upon cooling to room temperature, the filtrate afforded pale yellow crystals of **1**. Yield: 0.33 g (57%). M.p. >300 °C. Found: C, 64.33; H, 4.82; N, 9.90%. Calc. for $C_{30}H_{28}N_4O_3Zn$ (MW = 557.93 $gmol^{-1}$): C, 64.58; H, 5.06; N, 10.04%. IR (cm^{-1}): 1615w, 1599m, 1570s, 1494s, 1462s, 1420m, 1391s, 1366m, 1325s, 1105s, 827m, 796m, 744s, 486w. ^{1}H-NMR (DMSO-d_6): $\delta_{H;}$ 8.54-6.87 [br m, 20H, ArH], 2.25 [s, 6H, Me] ppm. ^{13}C NMR (DMSO-d_6): $\delta_{C;}$ 162.20, 149.53, 147.88, 145.59, 140.18, 139.13, 130.30, 129.88, 125.30, 121.84, 112.82, 110.17 [ArC], 20.87 [CH_3] ppm.

*2.2.2. Synthesis of $[Zn(L^{MeAQ})_2(Py)_2]\cdot C_6H_6$ (**2a**).* A slightly modified method to that used for the preparation of **1** was followed. $Zn(OAc)_2\cdot 2H_2O$ (0.21 g, 0.95 mmol) in methanol (10 mL) was added drop-wise to a stirred solution of HL^{MeAQ} (0.50 g, 1.90 mmol) in benzene (50 mL) at room temperature, which resulted in the immediate formation of a red-colored precipitate. The reaction mixture was heated to reflux for 3 h and then filtered while hot. The residue was washed with hot methanol (3 x 5 mL) to remove undesired materials and dried *in vacuo*. The dried solid was dissolved in hot chloroform (15 mL) containing pyridine (0.8 mL, 10 mmol) and filtered to remove any suspended particles. The filtrate was diluted with benzene (1 mL) and filtered while

hot. The filtrate, upon slow evaporation afforded dark red crystals. Yield: 0.49 g (62%). M.p. >300 °C. Found: C, 69.92; H, 4.75; N, 13.28%. Calcd. for $C_{48}H_{40}N_8O_2Zn$ (MW = 826.25 gmol^{-1}): C, 69.77; H, 4.88; N, 13.56%. IR (cm^{-1}): 1598m, 1573m, 1552m, 1497s, 1463s, 1408m, 1391m, 1329s, 1246s, 1213m, 1188m, 1169m, 1104s, 818w, 461w. ^{1}H NMR (DMSO-d_6): δ_H; 9.40 [br d, 2H, H-4], 8.69-8.57 [m, 8H, H-2, H-6, H-α(Py)], 8.13 [m, 2H, H-3], 7.90-7.70 [m, 10H, H-β(Py), H-γ(Py), H-2′,6′], 7.50-7.28 [m, 10H, H-3′,5′, C_6H_6], 6.92 [d, 2H, H-7], 2.37 [s, 6H, CH_3] ppm. ^{13}C NMR (DMSO-d_6): δ_C; 169.06, 151.63, 150.03, 145.98, 139.24, 138.96, 136.70, 135.12, 132.46, 130.19, 128.77, 124.42, 123.81, 122.21, 119.39, 113.52 [ArC], 21.36 [CH_3] ppm.

*2.2.3. Synthesis of [Zn(L^{MeAQ})$_2$(H_2O)$_2$] (**2b**).* An analogous method to that used for the preparation of **2a** was followed using $Zn(OAc)_2{\cdot}2H_2O$ (0.21 g, 0.95 mmol) and HL^{MeAQ} (0.50 g, 1.90 mmol). The dried solid was dissolved in hot chloroform (15 mL) containing 3-methylpyridine (1 ml, 10 mmol) and filtered. The filtrate upon slow evaporation yielded red orange crystals. Yield: 0.49 g (82%). M.p. >300 °C. Found: C, 61.25; H, 2.63; N, 13.86%. Calcd. for $C_{32}H_{28}N_6O_4Zn$ (MW = 625.97 gmol^{-1}): C, 61.40; H, 4.51; N, 13.43%. IR (cm^{-1}): 1600m, 1573m, 1555m, 1500s, 1468s, 1408s, 1390m, 1334s, 1258s, 1193m, 1172m, 1132m, 1103m, 814m, 789m, 462m. ^{1}H NMR (DMSO-d_6+$CDCl_3$): δ_H; 9.40 [br d, 2H, H-4], 8.74 [br d, 2H, H-2], 8.36 [d, 2H, H-6], 8.13 [m, 2H, H-3], 7.75 [m, 4H, H-2′,6′), 7.28 [m, 4H, H-3′,5′], 6.90 [d, 2H, H-7], 2.37 [s, 6H, CH_3] ppm. ^{13}C NMR (DMSO-d_6+$CDCl_3$): δ_C; 151.09, 149.59, 146.45, 145.49, 136.55, 134.72, 132.19, 129.48, 123.20, 122.89, 121.66, 118.78, 112.94 [ArC], 20.92 [CH_3] ppm.

*2.2.4. Synthesis of [Zn(L^{OMeAQ})$_2$(H_2O)$_2$] (**3**).* An analogous method to that used for the preparation of **2a** was followed using $Zn(OAc)_2{\cdot}2H_2O$ (0.20 g, 0.89 mmol) and HL^{OMeAQ} (0.50 g, 1.79 mmol). The dried solid was dissolved in hot chloroform (15 mL) containing pyridine (0.8 mL, 10 mmol) and filtered to remove any suspended particles. The filtrate was diluted with hexane (1 mL) and filtered while hot. The filtrate upon slow evaporation afforded red orange crystals of **3**. Yield: 0.51 g (86%). M.p. >300 °C. Found: C, 58.65; H, 4.43; N, 12.60%. Calcd. for $C_{32}H_{28}N_6O_6Zn$ (MW = 657.97 gmol^{-1}): C, 58.41; H, 4.29; N, 12.77%. IR (cm^{-1}): 1598m, 1573m, 1555m, 1499s, 1469s, 1431m, 1403m, 1393m, 1335s, 1293m, 1257s, 1192m, 1171m,

1151m, 1104m, 1024m, 837m, 789w, 464w. ^{1}H NMR (DMSO-d_6 + $CDCl_3$): δ_H; 9.37 [br d, 2H, H-4], 8.74 [br d, 2H, H-2], 8.08 [d, 2H, H-6], 7.81 [m, 4H, H-2′,6′), 7.67 [m, 2H, H-3], 6.98 [m, 4H, H-3′,5′], 6.92 [d, 2H, H-7], 3.81 [s, 6H, OCH_3] ppm. ^{13}C NMR (DMSO-d_6+$CDCl_3$): δ_C; 160.07, 152.37, 147.25, 145.43, 138.47, 136.27, 134.38, 129.56, 128.63, 123.26, 122.51, 113.98, 112.81 [ArC], 55.19 [OMe] ppm.

*2.2.5. Synthesis of [Zn(L^{EtAQ})$_2$(3-MePy)$_2$] (**4**).* An analogous method to that used for the preparation of **2a** was followed using $Zn(OAc)_2{\cdot}2H_2O$ (0.20 g, 0.90 mmol) and HL^{EtAQ} (0.50 g, 1.80 mmol). The dried solid was dissolved in hot benzene (10 mL) containing 3-methylpyridine (1 ml, 10 mmol) and filtered while hot. The filtrate upon slow evaporation afforded red crystals. Yield: 0.47 g (65%). M.p. >300 °C. Found: C, 68.85; H, 5.18; N, 14.23%. Calcd. for $C_{46}H_{42}N_8O_2Zn$ (MW = 804.24 gmol^{-1}): C, 68.70; H, 5.26; N, 13.93%. IR (cm^{-1}): 1598s, 1568s, 1498s, 1465s, 1403s, 1328s, 1248s, 1214w, 1191m, 1172m, 1135m, 1100m, 840m, 791m, 754w, 469w. ^{1}H NMR (DMSO-d_6): δ_H; 9.40 [br d, 2H, H-4], 8.71 [br d, 2H, H-2], 8.41-8.37 [m, 4H, Hα (3-MePy)], 8.13 [d, 2H, H-6], 7.80 [m, 6H, H-3 and H-2′,6′), 7.60 [d, 2H, Hγ (3-MePy)], 7.34-7.28 [m, 6H, H-3′,5′, Hβ (3-MePy)], 6.92 [d, 2H, H-7], 2.64 (q, 4H, CH_2), 2.26 [s, 6H, CH_3 (3-MePy)], 1.19 (t, 6H, CH_3) ppm. ^{13}C NMR (DMSO-d_6): δ_C; 168.40, 151.35, 149.66, 146.56, 145.59, 145.03, 138.45, 136.77, 134.66, 133.14, 132.09, 128.82, 128.49, 123.42, 123.31, 121.79, 118.91, 113.02 [ArC], 27.95 [CH_2], 17.87 [CH_3 (3-MePy)], 15.47 [CH_3] ppm.

*2.2.6. Synthesis of [Zn(L^{OEtAQ})$_2$(4-MePy)$_2$]·0.5C_6H_7N (**5a**).* An analogous method to that used for the preparation of **2a** was followed using $Zn(OAc)_2{\cdot}2H_2O$ (0.19 g, 0.85 mmol) and HL^{OEtAQ} (0.50 g, 1.70 mmol). The dried solid was dissolved in hot DMF (6 mL) containing 4-methylpyridine (1 ml, 10 mmol) and filtered while hot. The filtrate was diluted with toluene (1 mL) and filtered, which upon slow evaporation afforded dark red crystals. Yield: 0.51 g (34%). M.p. >300 °C. Found: C, 67.28; H, 5.26; N, 13.04%. Calcd. for $C_{98}H_{91}N_{17}O_8Zn_2$ (MW = 1765.61 gmol^{-1}): C, 66.66; H, 5.19; N, 13.49%. IR (cm^{-1}): 1597s, 1570s, 1496s, 1464s, 1434m, 1400s, 1325s, 1242s, 1190m, 1150m, 1101m, 1046m, 922w, 836m, 791m, 766m, 722w, 463w. ^{1}H NMR (DMSO-d_6): δ_H; 9.31 [br d, 2H, H-4], 8.63 [br d, 2H, H-α(Py)], 8.50-8.60 [m, 7H, H-α(Py), H-2′,6′], 8.00 [br d, 2H, H-2], 7.76 [d, 2H, H-6], 7.15-7.00 [m, 8H, H-β(Py), H-3′,5′], 6.96 [m, 3H, H-3, H-β(Py)], 6.80 [d, 2H, H-7], 4.00 [q, 4H, CH_2], 3.27 [s, 7.5H, CH_3 (4-MePy)], 1.25 [t, 6H,

CH_3] ppm. ^{13}C NMR (DMSO-d_6): δ_C; 167.29, 159.70, 149.23, 147.55, 146.82, 138.22, 134.85, 131.47, 129.14, 128.05, 124.65, 123.77, 123.38, 118.42, 114.75, 112.85 [ArC], 63.37 [CH_2], 20.39 [CH_3 (4-MePy)], 14.60 [CH_3] ppm.

*2.2.7. Synthesis of [Zn(L^{OEtAQ})$_2$(H_2O)$_2$] (**5b**).* An analogous method to that used for the preparation of **2a** was followed using Zn(OAc)$_2$·2H_2O (0.19 g, 0.85 mmol and HL^{OEtAQ} (0.50 g, 1.70 mmol). The dried solid was dissolved in hot chloroform (15 mL) containing pyridine (0.8 mL, 10 mmol) and filtered to remove any suspended particles. The filtrate was diluted with hexane (1 mL) and filtered while hot, which upon slow evaporation afforded red crystals of the desired product. Yield: 0.51 g (87%). M.p. >300 °C. Found: C, 59.35; H, 4.60; N, 12.50%. Calcd. for $C_{34}H_{32}N_6O_6Zn$ (MW = 686.02 gmol^{-1}): C, 59.53; H, 4.70; N, 12.25%. IR (cm^{-1}): 1598m, 1573m, 1555w, 1499s, 1469s, 1431w, 1394m, 1335s, 1255s, 1192w, 1172m, 1150m, 1103m, 1043m, 838w, 466w. ^{1}H NMR (DMSO-d_6): δ_H; 9.41 [br d, 2H, H-4], 8.72 [br d, 2H, H-2], 8.09 [d, 2H, H-6], 8.00-7.60 [m, 6H, H-3 and H-2′,6′), 7.06 [m, 4H, H-3′,5′], 6.88 [d, 2H, H-7], 4.10 [q, 4H, CH_2], 1.35 (t, 6H, CH_3) ppm. ^{13}C NMR (DMSO-d_6): δ_C; 167.85, 159.43, 147.16, 145.59, 138.46, 134.74, 131.99, 128.62, 123.40, 123.16, 118.40, 114.75, 112.83 [ArC], 63.37 [CH_2], 14.61 [CH_3] ppm.

*2.2.8. Synthesis of [Zn(L^{NMe2AQ})$_2$(Py)$_2$]·1.5C_6H_6·H_2O (**6**).* An analogous method to that used for the preparation of **2a** was followed using Zn(OAc)$_2$·2H_2O (0.19 g, 0.85 mmol) and HL^{NMe2AQ} (0.50 g, 1.71 mmol). The dried solid was dissolved in hot benzene (10 mL) containing pyridine (0.8 mL, 10 mmol) and filtered to remove any suspended particles. The filtrate was diluted with chloroform (2 mL) and filtered while hot, which upon slow evaporation afforded dark red crystals of **6**. Yield: 0.47 g (58%). M.p. >300 °C. Found: C, 67.81; H, 5.10; N, 15.06%. Calcd. for $C_{53}H_{51}N_{10}O_3Zn$ (MW = 941.41 gmol^{-1}): C, 67.62; H, 5.46; N, 14.88%. IR (cm^{-1}): 1595s, 1572m, 1565m, 1493s, 1459s, 1443m, 1406m, 1385w, 1364m, 1321s, 1257m, 1227m, 1155m, 1095m, 945w, 820m, 792, 700w, 484w. ^{1}H NMR (DMSO-d_6): δ_H; 9.31 [br d, 2H, H-4], 8.68 [br d, 2H, H-2], 8.50 [d, 4H, H-α(Py)], 7.96 [d, 2H, H-6], 7.80-7.60 [m, 10H, H-β(Py), H-γ(Py), H-2′,6′], 7.40-7.20 [m, 11H, H-3′,5′, C_6H_6], 6.83 [d, 2H, H-β(Py)], 6.73 [m, 4H, H-3,H-7], 2.93 [s, 12H, N(CH_3)$_2$] ppm. ^{13}C NMR (DMSO-d_6): δ_C; 166.01, 150.52, 148.99, 145.09, 143.28, 138.03,

135.77, 134.31, 127.75, 127.64, 123.43, 122.96, 122.20, 117.01, 112.16, 111.25 [ArC], 54.55 [$N(CH_3)_2$] ppm.

*2.2.9. Synthesis of [Zn(L^{CAQ})$_2$(Py)] (**7**).* An analogous method to that used for the preparation of **2a** was followed using $Zn(OAc)_2{\cdot}2H_2O$ (0.19 g, 0.88 mmol) and HL^{CAQ} (0.50 g, 1.76 mmol). The dried solid was dissolved in hot chloroform (10 mL) containing pyridine (0.4 ml, 5 mmol). The filtrate was diluted with benzene (2 mL) and filtered while hot, which upon slow evaporation afforded dark red crystals of **7**. Yield: 0.51 g (81%). M.p. >300 °C. Found: C, 58.92; H, 3.20; N, 13.99%. Calcd. for $C_{35}H_{23}Cl_2N_7O_2Zn$ (MW = 709.87 $gmol^{-1}$): C, 59.22; H, 3.27; N, 13.81%. IR (cm^{-1}): 1598m, 1573m, 1557m, 1498m, 1465s, 1423w, 1408m, 1388m, 1328s, 1298w, 1246m, 1221w, 1188w, 1170w, 837w, 739w, 470w. ^{1}H NMR (DMSO-d_6+$CDCl_3$): δ_H; 9.38 [br d, 2H, H-4], 8.75 [br d, 2H, H-2], 8.65-8.40 [m, 5H, H-α(Py), H-2′,6′], 8.15 [d, 1H, H-α(Py)], 7.82 [d, 2H, H-6], 7.69 [m, 3H, H-3, H-γ(Py)], 7.44 [m, 1H, H-β(Py)], 7.40-7.20 [m, 5H, H-β(Py), H-3′,5′], 6.94 [d, 2H, H-7] ppm. ^{13}C NMR (DMSO-d_6+$CDCl_3$): δ_C; 151.84, 149.36, 146.72, 145.52, 139.63, 135.90, 134.11, 132.25, 130.26, 128.94, 128.12, 123.66, 123.10, 121.18, 118.81, 112.40 [ArC] ppm.

*2.2.10. Synthesis of [Zn(L^{BAQ})$_2$(Py)] (**8**).* An analogous method to that used for the preparation of **2a** was followed using $Zn(OAc)_2{\cdot}2H_2O$ (0.17 g, 0.76 mmol) and HL^{BAQ} (0.50 g, 1.52 mmol). The dried solid was dissolved in hot chloroform (10 mL) containing pyridine (0.4 ml, 5 mmol). The filtrate was diluted with benzene (2 mL) and filtered while hot, which upon slow evaporation afforded dark red crystals of **8**. Yield: 0.47 g (78%). M.p. >300 °C. Found: C, 52.76; H, 3.12; N, 12.28%. Calcd. for $C_{35}H_{23}Br_2N_7O_2Zn$ (MW = 798.79 gmol-1): C, 52.63; H, 2.90; N, 12.27%. IR (cm^{-1}): 1598m, 1572m, 1557m, 1499s, 1465s, 1422w, 1407m, 1327s, 1250s, 1219w, 1188m, 1170w, 1134w, 1103w, 1064w, 836w, 738w, 699w, 470w. ^{1}H NMR (DMSO-d_6+$CDCl_3$): δ_H; 9.38 [br d, 2H, H-4], 8.74 [br d, 2H, H-2], 8.65-8.40 [m, 5H, H-α(Py), H-2′,6′], 8.15 [d, 1H, H-α(Py)], 7.80-7.50 [m, 5H, H-6, H-3, H-γ(Py)], 7.44 [m, 1H, H-β(Py)], 7.50-7.20 [m, 5H, H-β(Py), H-3′, 5′], 6.94 [d, 2H, H-7] ppm. ^{13}C NMR (DMSO-d_6+$CDCl_3$): δ_H; 151.37, 149.34, 146.52, 145.25, 139.78, 135.87, 134.34, 131.84, 130.40, 128.55, 128.12, 123.63, 123.37, 121.58, 118.71, 112.38 [ArC] ppm.

2.3. X-ray crystallography

Intensity data for compounds **1**-**8** were collected at ambient temperature with Mo-K_α radiation (λ = 0.71073 Å, monochromator: graphite) on an Agilent Technologies Xcalibur diffractometer equipped with an EOS CCD area detector. The measured intensities were reduced to F^2 and corrected for absorption using spherical harmonics (CryAlisPro) [56]. Intensities were corrected for Lorentz and polarization effects. Structure solution, refinement and data output were performed with the OLEX2 program package [57] using SHELXTL [58a] and SHELXL-2014 [58b]. Non-hydrogen atoms were refined anisotropically. C-H hydrogen atoms were placed in geometrically calculated positions using the riding model. The hydrogen atoms of water molecules were treated with AFIX 6 (compound **1**) or a distance restraint (0.850±0.001 Å for compounds **2b**, **3**, **5b** and **6**). U_{iso} factors for O_w-H hydrogen atoms were restrained to 1.5U_{iso}(O). DIAMOND was used for the creation of figures [59].

With exception of **6**, the molecular structures of the remaining compounds exhibited crystallographic symmetry (2-axis for **1**, **7** and **8**; inversion symmetry for **2a**, **2b**, **3**, **4**, **5a**, and **5b**). In addition, the asymmetric unit of compound **5a** comprises two crystallographically independent molecule halves. The crystal structures of compounds **1** (H_2O), **2a** (benzene), **5a** (4-methylpyridine) and **6** (benzene and H_2O) contain solvate molecules. In **2a**, benzene molecules were disordered over crystallographic inversion centers and were refined using the AFIX66, SIMU and ISOR instructions implemented in the SHELXL program. In the crystal structure of **6** with one and a half benzene molecules in the asymmetric unit, AFIX66, SIMU, DELU and ISOR commands were used during the refinement. Finally, the disorder of the N-C_6H_4-R fragments in **4**, **7** and **8** and, additionally, the 3-methylpyridine ligands in **4** were refined using AFIX66, SIMU and EADP. Compound **1** crystallized in a chiral space group and refinement of the absolute structure parameter yielded a value, which confidently confirms that the refined model corresponds to the true enantiomorph (Table 1). Crystallographic data for compounds **1**-**8** reported in this paper have been deposited with the Cambridge Crystallographic Data Centre (CCDC) as supplementary publication nos. CCDC-1811363-CCDC-1811372. These data can be obtained free of charge via www.ccdc.cam.ac.uk/getstructures.

2.4. Synthesis of ZnO nanoparticles (NPs)

The dried zinc precursor compound **2a** (0.054 g) was transferred to a platinum crucible and gradually heated in a muffle furnace at a rate of 10 °C/min until the temperature reached 600 °C. The crucible was heated for 4 h at 600 °C and then cooled gradually to room temperature. The calcinated ZnO (0.005 g) was suspended in double-distilled water (20 mL) and the mixture was exposed to high-intensity ultrasound irradiation under ambient air for 30 min., giving a uniform white suspension. After cooling to room temperature, the particles were separated by centrifugation at 6000 rpm. The procedure was repeated three times by re-dispersing the sample in acetone. Acetone was separated by decantation, the ZnO residue was dried in hot air oven for an hour at 120 °C and stored in vacuum. Dried sample was used directly for the measurement of PXRD pattern. For imaging studies, the dried ZnO NPs were re-dispersed in ethanol.

2.5. In vitro antimicrobial assay

The antimicrobial activity of pro-ligands HL^{Q}/HL^{XAQ} and the corresponding zinc(II) compounds **1**-**8** was tested against five indicator bacterial strains i.e. *Escherichia coli* MTCC 730, *Streptococcus pyogenes* MTCC 1925, *Klebsiella pneumoniae* MTCC 109, *Bacillus cereus* MTCC 430 and *Salmonella enterica* MTCC 735, according to the agar-well diffusion method [60].

The stock solutions for pro-ligands HL^{Q}/HL^{XAQ} and the corresponding zinc(II) compounds **1**-**8** were prepared freshly in DMSO prior to use. The stock concentration of the tested sample was ~10,000 µg/mL. Muller-Hilton agar plates were swabbed with bacterial cell suspension of the indicator bacterial strains adjusted to 1.5 x 10^8 colony forming units (CFU)/ml. Then, the agar surface was bored by using a sterilized cork borer to generate wells of 5 mm diameter, which were filled with a 100 µL aliquot of the corresponding test compound solution. The broad-spectrum antibiotic chloramphenicol (30 mcg) disc was used as positive control and a DMSO solution as negative control. Plates were incubated at 37 °C for 24 h and the inhibition zones (mm) formed around the wells were measured using a Vernier caliper. For each organism, the experiments were conducted in triplicate and the results were recorded as the mean diameter of the zones of inhibition.

3. Results and discussion

3.1. Synthesis and spectroscopic characterization

The pro-ligands 5-[(4-(X)-phenyl)-1-diazenyl]quinolin-8-ol (HL^{XAQ}) with X = Me, OMe, Et, OEt, NMe_2, Cl and Br were synthesized following literature procedures [49a,49b,53] and characterized by microanalytical methods, IR and NMR spectroscopy. The respective Zn(II) compounds were prepared by reacting in 1:2 molar ratio of a solution of $Zn(OAc)_2 \cdot 2H_2O$ in methanol either with HL^{Q} dissolved in methanol or HL^{XAQ} dissolved in benzene. In all cases, the immediate formation of a precipitate was noticed. Characterization of the isolated precipitates revealed compounds of compositions $[Zn(L^{Q})_2]$ and $[Zn(L^{XAQ})_2]$, respectively. The solids were amorphous and insoluble in most of the common organic solvents even after prolonged heating. Solubility was detected in DMSO, pyridine and pyridine derivatives such as methylpyridines. Crystallization experiments with $[Zn(L^{Q})_2]$ and $[Zn(L^{XAQ})_2]$ using pure DMSO or a combination with other common solvents invariably afforded amorphous materials. However, when a large excess of pyridine (Py), 3-methylpyridine (3-MePy) or 4-methylpyridine (4-MePy) was added to a solution of the zinc(II) compounds in benzene, chloroform, ethanol, DMF or a solvent mixture with either of these solvents, the isolation of crystalline zinc(II) compounds, in which either Py (**2a**, **6**, **7**, **8**), 3-MePy (**4**), 4-MePy (**1**, **5a**) or H_2O (**2b**, **3**, **5b**) was coordinated to the zinc atoms, became feasible. Of these, compounds **1**, **2a**, **5a** and **6** crystallized as solvates with H_2O (**1**), benzene (**2a**), 4-MePy (**5a**) and benzene/H_2O (**6**), see Table 1. The presence of water in compounds **2b**, **3**, **5b** and **6** is attributed to traces of water in the solvents and reagents used for the crystallization experiments. It should be mentioned that complexation experiments were carried out under identical conditions with pyridine and all three monomethyl pyridine derivatives (picolines), i.e. 2-/3-/4-methylpyridine, but for each ligand only a specific N-base or water provided a crystalline product, as detailed in Scheme 1.

In compounds **1**-**6**, the adduct formation of $[Zn(L^{Q})_2]$ and $[Zn(L^{XAQ})_2]$ generated six-coordinate structures with the participation of two mole equivalents of pyridine, 3-MePy, 4-MePy or water. On the contrary, compounds **7** and **8** assume a five-coordinate geometry, even if the concentration of pyridine employed for the reaction was increased from 5 to 10 mmol, indicating that the molecular structure variation is influenced by crystal packing effects.

The formulations of the compounds were ascertained from the microanalytical data, the $^{1}H/^{13}C$ NMR and are further supported by the results of single-crystal X-ray diffraction analyses. The infrared spectra of compounds **1-8** are very similar and the most pertinent IR frequencies are included in the experimental section. The ^{1}H and ^{13}C NMR signals for the pro-ligands HL^{XAQ} were assigned by using 2D ^{1}H-^{1}H-correlation spectroscopy (COSY) as well as heteronuclear single-quantum correlation (HSQC) and heteronuclear multiple-bond connectivity (HMBC) experiments [49a]. Compounds **1-8** were characterized in solution by ^{1}H and ^{13}C NMR spectroscopy, either in DMSO-d_6 or a solvent mixture of DMSO-d_6 and $CDCl_3$ (1:1, v/v). The ligand signal assignments of HL^{Q} and HL^{XAQ} were subsequently extrapolated to the zinc(II) compounds, owing to the data similarity. It is worth mentioning that the Zn(II) compounds **1-8** displayed broad ^{1}H NMR signals and did not show much difference in the chemical shifts when compared within the series studied herein, indicating that the changes in the magnetic environment of the metal ions are insignificant. The ^{1}H and ^{13}C NMR spectra of **1-8** displayed the expected signals for the metal- coordinated L^{Q}/L^{XAQ} ligand skeletons and coordinated pyridine/3-methylpyridine/4-methylpyridine in **1**, **2a**, **4**, **5a** and **6-8**.

The photophysical properties of the tetrahedral zinc compounds $[Zn(L^{Q})_2]$ and $[Zn(L^{XAQ})_2]$ were thoroughly studied in previous reports [46,52,53]. As expected, the zinc compound with HL^{Q} i.e. $[Zn(L^{Q})_2(4\text{-}MePy)_2]\cdot H_2O$ (**1**) exhibited different experimental absorption and emission features in comparison to compounds **2-8** that contain 5-substituted diazenyl ligands. The UV-Vis absorption spectra of HL^{Q}, HL^{XAQ} and the corresponding zinc(II) compounds **1-8** in DMSO are depicted in Fig. S1, ESI†. Table S1 summarizes the most relevant characteristics of the UV-Vis data. The absorption spectra of **2-8** are comparable with those measured for the tetrahedral bis(5-(aryl)-1-diazenyl]quinolin-8-olato)zinc(II) compounds, $[Zn(L^{XAQ})_2]$, exhibiting only compound with slight changes in the absorption maximum. This is because the electronic excitation does not involve transitions with the participation of metal-based molecular orbitals, since the $3d^{10}$ shell is too low and the empty 4s and 4p orbitals are too high in energy [52,53]. Pro-ligands, HL^{XAQ} showed very similar absorption spectra and were non-emissive except for HL^{NMe2AQ}. Emission experiments with λ_{ex} = 425 nm for the five and six-coordinate zinc(II) compounds **2-8** revealed the same result (non-emissive) except for compound **6** (λ_{em} = 525 nm), which contain a strong π−electron donor group -NMe_2 and the emission spectrum resembles that of the pro-ligand HL^{NMe2AQ} (Fig. S2 (a), ESI†). On the contrary, in DMSO solution, octahedral

$[Zn(L^{Q})_2(4\text{-}MePy)_2]\cdot H_2O$ (**1**) gave a significantly improved fluorescence quantum yield (ϕ = 0.25), when compared to the tetrahedral analog $[Zn(L^{Q})_2]$, signaling enhanced electron-transporting properties (Fig. S2 (b), ESI†). The highly fluorescent performance of compound **1** is also detected in the solid-state fluorescence spectrum with λ_{em} 500 nm (Fig. S2 (b), ESI†).

3.2. Description of the X-ray crystal structures

Crystals of the zinc(II) compounds, $[Zn(L^{Q})_2(4\text{-}MePy)_2]\cdot H_2O$ **1** (ethanol/4-methylpyridine), $[Zn(L^{MeAQ})_2(Py)_2]\cdot C_6H_6$ **2a** (chloroform/pyridine/benzene), $[Zn(L^{MeAQ})_2(H_2O)_2]$ **2b** (chloroform/3-methylpyridine), $[Zn(L^{OMeAQ})_2(H_2O)_2]$ **3** (chloroform/pyridine/hexane), $[Zn(L^{EtAQ})_2(3\text{-}MePy)_2]$ **4** (benzene/3-methylpyridine), $[Zn(L^{OEtAQ})_2(4\text{-}MePy)_2]\cdot 0.5C_6H_7N$ **5a** (DMF/4-methylpyridine), $[Zn(L^{OEtAQ})_2(H_2O)_2]$ **5b** (chloroform/pyridine/hexane), $[Zn(L^{NMe2AQ})_2(Py)_2]\cdot 1.5C_6H_6\cdot H_2O$ **6** (benzene/pyridine/chloroform), $[Zn(L^{CAQ})_2(Py)]$ **7** (chloroform/pyridine/benzene) and $[Zn(L^{BAQ})_2(Py)]$ **8** (chloroform /pyridine/benzene) suitable for single-crystal X-ray structure determination were obtained by slow evaporation of solutions of the respective compounds. Crystal data, data collection parameters and convergence results are listed in Table 1, while a comparison of selected bond distances and angles is shown in Tables 2 and 3. Perspective views of the molecular structures are shown in Figs. 1-7, while views of the asymmetric units of the crystal structures including displacement ellipsoids are shown in Fig. S3, ESI†.

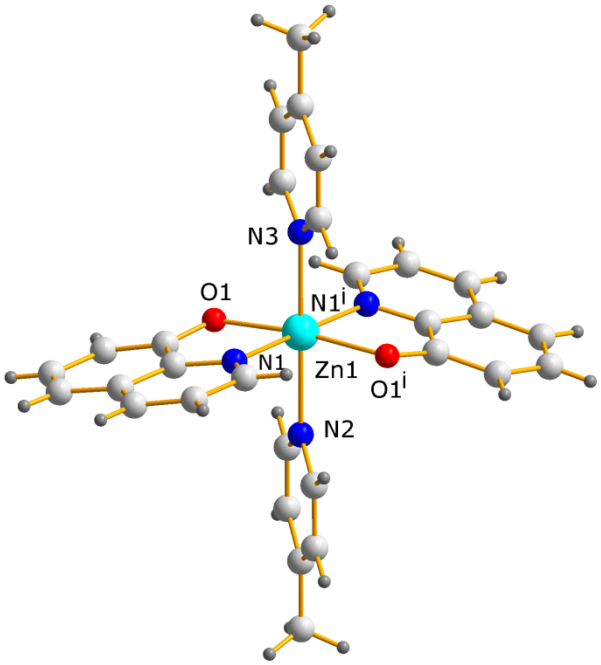

Fig. 1. Perspective view of the molecular structure of compound **1** with partial atom labeling scheme. Symmetry operator: (i) 1-y, 1-x, 0.75-z.

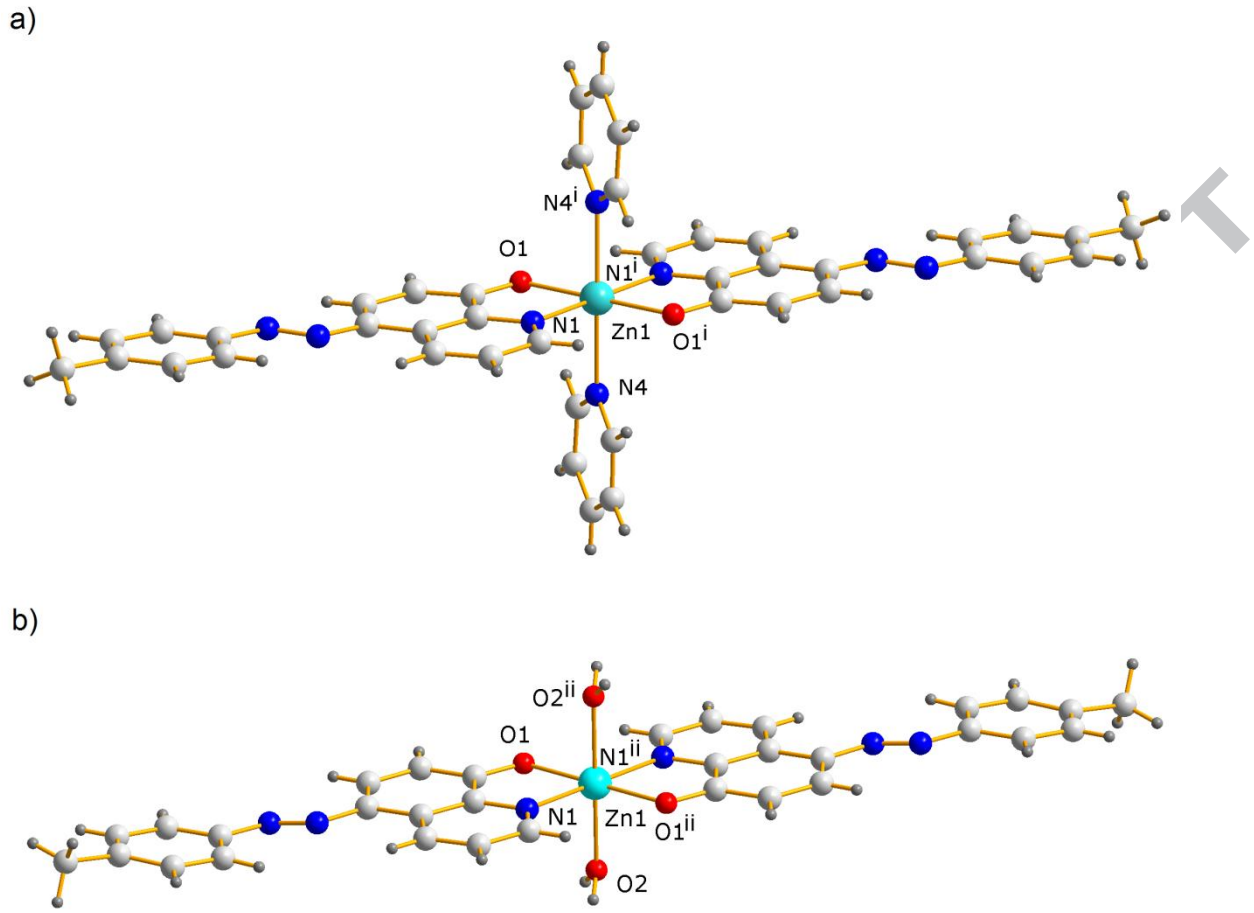

Fig. 2. Perspective views of the molecular structures of compounds (a) **2a** and (b) **2b** with partial atom labeling schemes. Symmetry operators: (i) 1-x, -y, 2-z; (ii) 1.5-x, 1.5-y, 0.5-z.

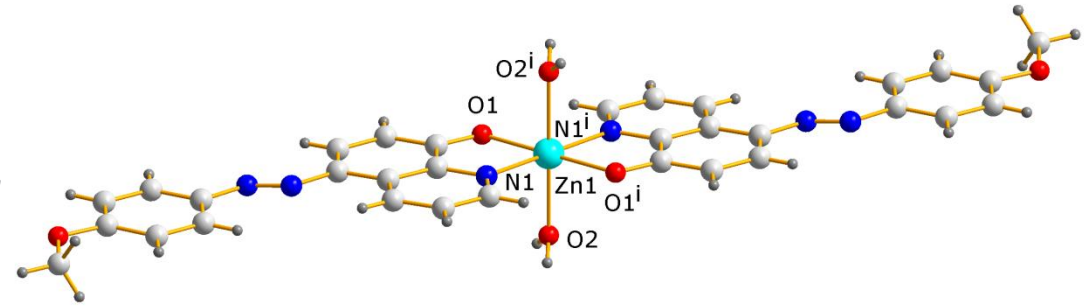

Fig. 3. Perspective view of the molecular structure of compound **3** with partial atom labeling scheme. Symmetry operator: (i) 1-x, 2-y, 1-z.

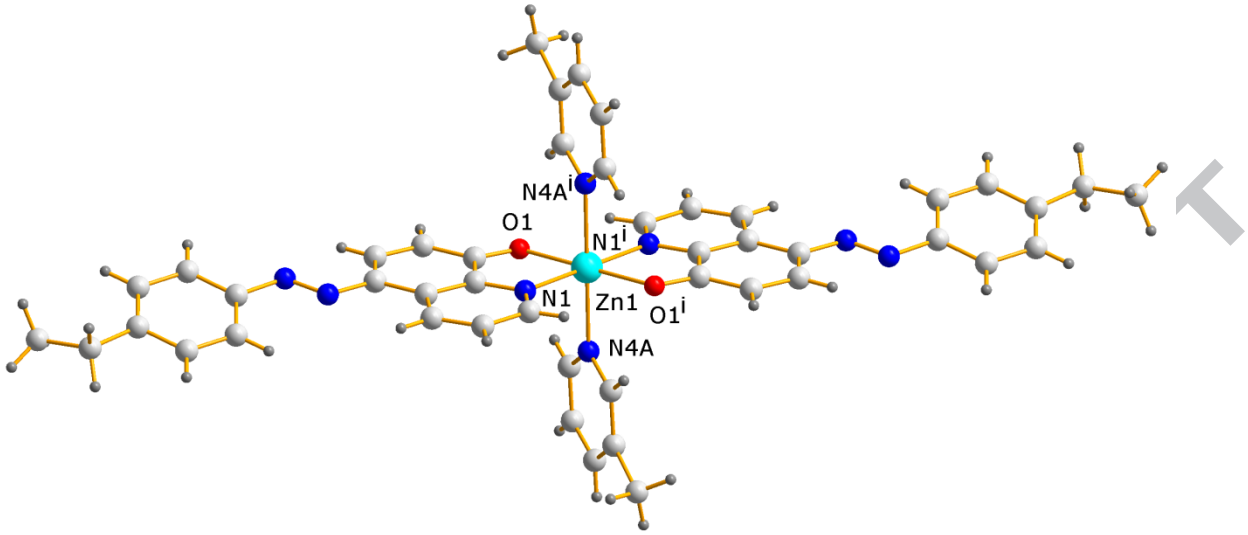

Fig. 4. Perspective view of the molecular structure of compound **4** with partial atom labeling scheme. Symmetry operator: (i) 1-x, 1-y, 2-z. For clarity, disorder is not shown.

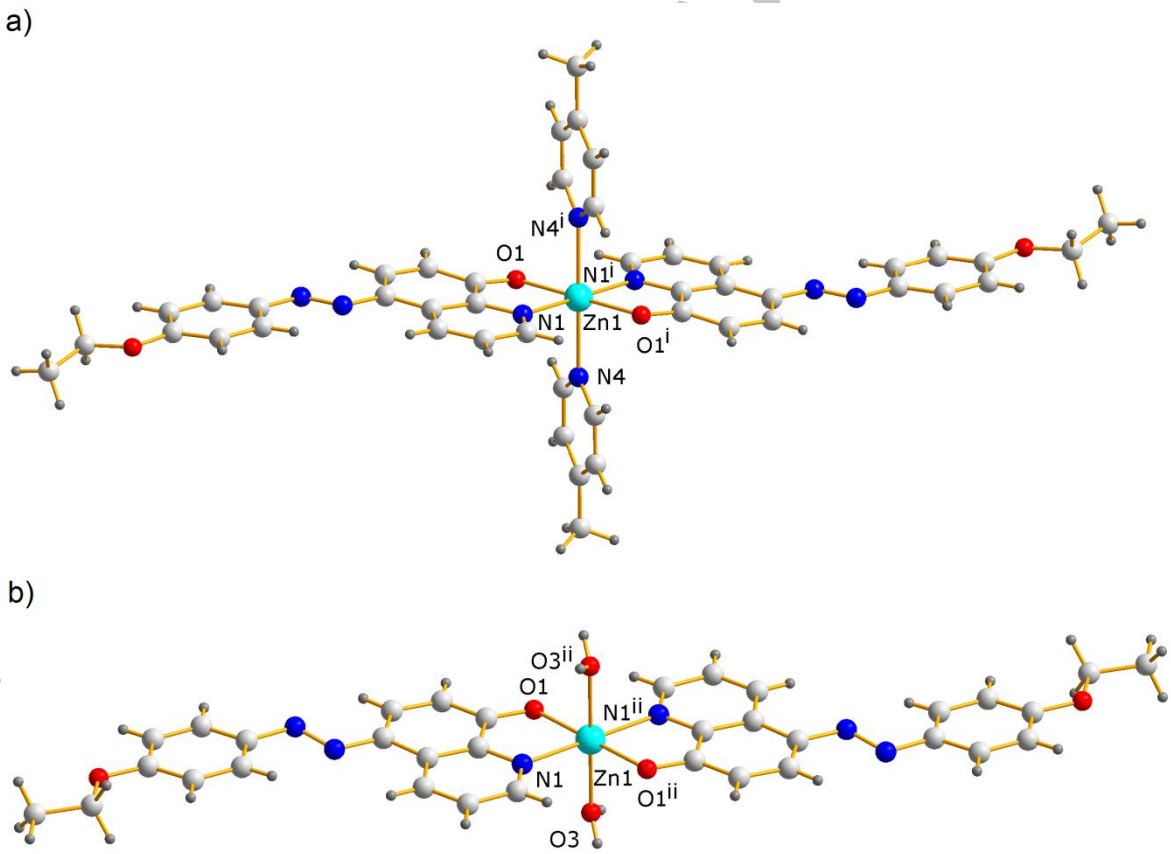

Fig. 5. Perspective views of the molecular structures of compounds (a) **5a** and (b) **5b** with partial atom labeling schemes. Symmetry operators: (i) -x, 1-y, 1-z; (ii) 2-x, -y, 1-z.

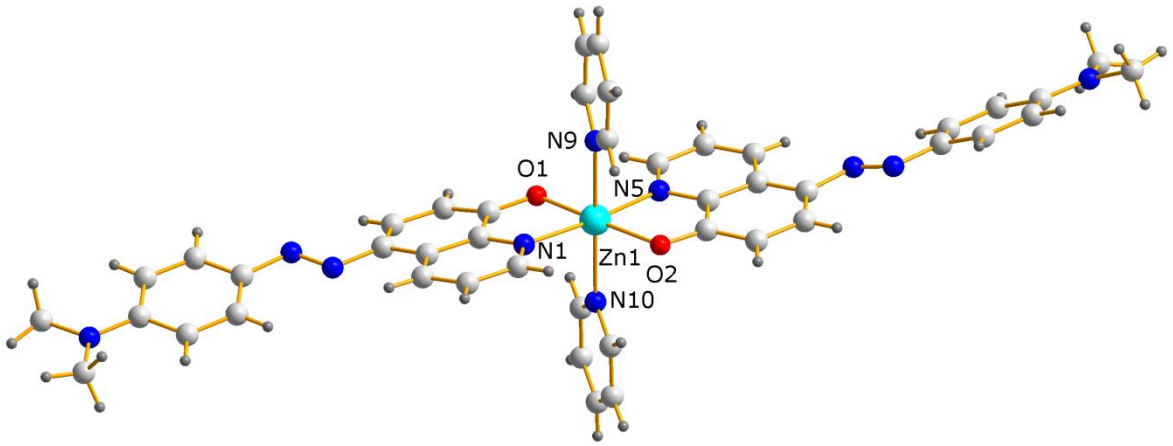

Fig. 6. Perspective view of the molecular structure of compound **6** with partial atom labeling scheme.

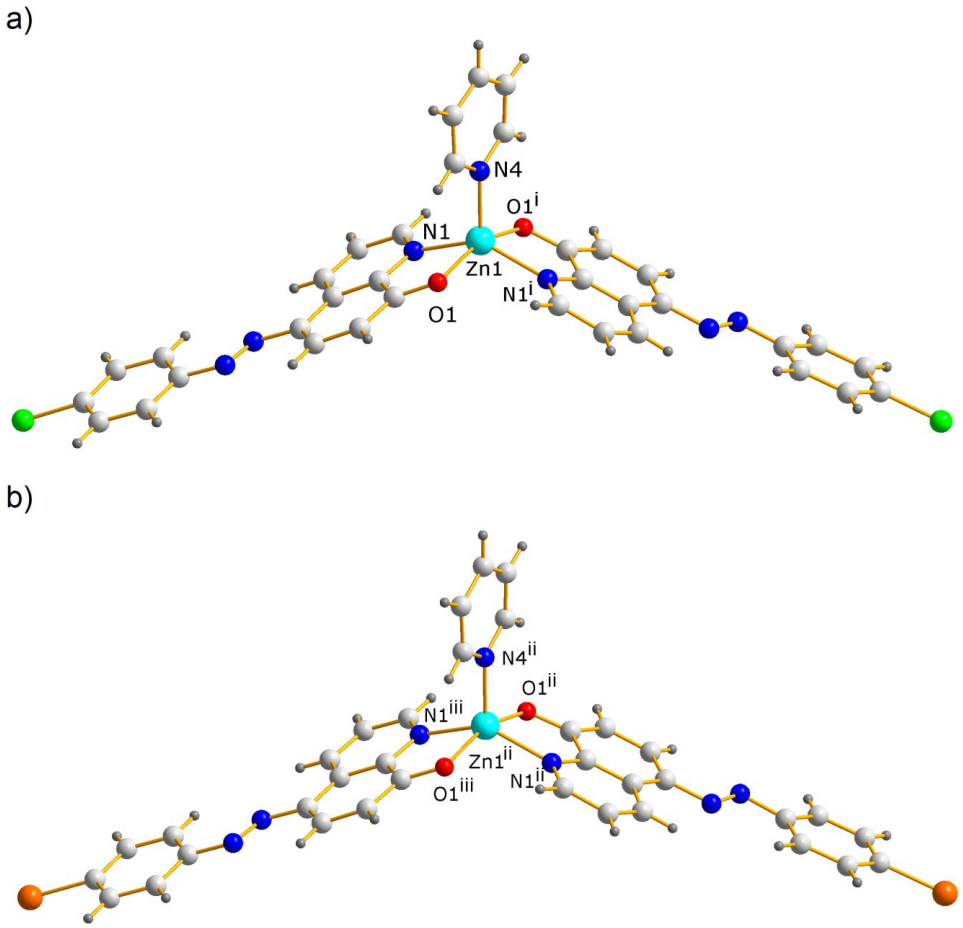

Fig. 7. Perspective views of the molecular structures of compounds (a) **7** and (b) **8** with partial atom labeling schemes. Symmetry operators: (i) 0.5-x, y, 1-z; (ii) 1-x, 1-y, 2-z; (iii) x, 1-y, 0.5+z. For clarity, disorder is not shown.

The molecular structure analysis of the SCXRD data reveals closely related coordination geometries for compounds **1**-**6**, in which the zinc atoms are embedded either in a ZnO_2N_4 (**1**, **2a**, **4**, **5a**, **6**) or a ZnO_4N_2 (**2b**, **3**, **5b**) polyhedron, depending whether the base coordinated to $[ZnL^{Q})_2]$ or $[Zn(L^{XAQ})]_2$ is a pyridine derivative or water. In all seven compounds, the quinolin-8-olate ligands occupy the equatorial positions with mutual *trans*-orientation of the phenoxide oxygen and quinoline nitrogen atoms. As a consequence, the Py and H_2O ligands are in the axial position, exhibiting significantly longer Zn–N and Zn–O distances with differences in the range of 0.15–0.22 Å for $\Delta d(Npy–N_{aquin})$ and 0.11–0.12 Å for $\Delta d(O_w–O_{quin})$. Except for **6**, the molecular structures of **1**-**5** exhibit crystallographic symmetry (2-axis for **1**; inversion symmetry for **2a**, **2b**, **3**, **4**, **5a**, and **5b**). The presence of symmetry in **1**, **2a**, **2b**, **3**, **4**, **5a** and **5b** restraints the N_{py}–Zn–Npy and Ow–Zn–Ow bond angles to 180.0° and for compounds **2a**, **2b**, **3**, **4**, **5a** and **5b**, additional bond angles N_{quin}–Zn–N_{quin} and O_{quin}–Zn–O_{quin} attain the same value. The coordination environments are significantly distorted from an ideal octahedral polyhedron owing to the involvement of L^{Q}/L^{XAQ} ligands in the formation of chelate ring (Table 3). The O_{quin}–Zn–N_{quin} bond angles within the chelate rings are significantly smaller than 90.0° and range from 80.27(10) to 81.19(7)° in close relationship to previously reported and related zinc(II) compounds [61]. As a consequence, the interligand O_{quin}–Zn–N_{quin} bond angles are significantly increased with values of 98.81(7)–99.63(8)° for **1**, **2a**, **2b**, **3**, **4**, **5a** and **5b** and 93.33(11)°/105.93(11)° for the asymmetric complex **6**. The bond angles with the axial substituents are close to 90.0° for **1**-6 and the deviations from this value do no exceed 5° (Table 3).

The five-coordinate zinc compounds **7** and **8** comprise distorted square-pyramidal geometries with the pyridine ligands in apical position. The L^{XAQ} ligands are trans-oriented, but in this case the Zn–N distances with the N_{py} atoms are significantly shorter, 2.013(5) and 2.035(4) Å when compared with Zn–N_{quin} nitrogen atoms, 2.092(3) and 2.102(3) Å. As expected, the Zn–N_{quin} and Zn–O_{quin} distances in **7**-**8** are significantly shorter than for the six-coordinate analogs (Table 2).

A search of the Cambridge Structural Database (CSD) revealed 17 entries for compounds of composition $[M(L^{Q}/L^{XAQ})_2]$ (M are first row transition metals) [61]. Interestingly, all have square-planar molecular structures with trans-coordination of the quinolin-8-olate ligands.

Among five six-coordinate compounds of composition $[M(L^{XQ})_2(H_2O)_2]$, cis-coordination of the two water molecules was observed only in the structure of $[Co(L^{Q})_2(H_2O)_2]$. The remaining compounds comprise two trans-coordinated ligand molecules in the equatorial plane, while the two water molecules occupy axial positions, as for **2b**, **3** and **5b**.

3.3. Supramolecular structure analysis

As mentioned in the introduction, π–stacking interaction are relevant for the electron-transport and optical properties of metal compounds derived from quinolin-8-olate ligands including $[Zn(L^{Q})_2]$ [36,37]. In view of this, it was thought worthwhile to analyze the influence of the substituents at the periphery of the L^{Q}/L^{XAQ} ligands and the base coordinated to the zinc(II) metal center and hence the supramolecular interactions in the crystal structures of **1**–**8** were examined in this section.

Pyridine adduct of tetrahedral $[Zn(L^{Q})_2]$ viz., $[Zn(L^{Q})_2(Py)_2]\cdot H_2O$ (**1**), did not exhibit π–stacking interactions in the solid state structure while the crystal structures of the remaining members of the series (**2-8**) are significantly influenced by π–π contacts, giving mostly 1D or 2D π–stacked assemblies. This difference is originated mainly by the significantly enhanced π–electron system of L^{XAQ} compared to unsubstituted quinolin-8-olate L^{Q}. From the molecular structure perspective, compounds **2-8** can be divided into three groups. Group I comprises of four compounds with approximate octahedral geometry and two pyridine-bases coordinated to the metal center: **2a** (X = Me, base = Py); **4** (X = Me, base = 3-MePy); **5a** (X = OEt, base = 4-MePy); **6** (X = NMe_2, base = Py). Group II is composed of three compounds with similar coordination geometry, but coordination of H_2O instead of the pyridine base: **2b** (X = Me, base = H_2O); **3** (X = OMe, base = H_2O); **5b** (X = OEt, base = H_2O). Finally, group III is constituted by two compounds with distorted square-pyramidal geometries and pyridine as base: **7** (X = Cl, base = Py); **8** (X = Br, base = Py). Therefore, the crystal structures are analyzed according to this classification.

*Group I (**2a**, **4**, **5a** and **6**)*

Compounds **2a**, **4** and **6** have similar supramolecular characteristics, particularly concerning the π–stacking interactions. In this context, the crystal structures of **2a** and **4** are structurally closely

related, albeit compound **2a** crystallized as benzene solvate while **4** is solvent-free. The central motif in **2a** and **4** consists of staircase-shaped 1D strands, which are stabilized by π–π interactions occurring mainly between the terminal $–C_6H_4X$ moieties of the metal-coordinated ligands and the diazo functional groups. As representative example, Fig. 8 shows the assembly found in **2a** with an interplanar distance of 3.56 Å. Neighboring π–stacked 1D strands are connected into 2D layers parallel to (-1 1 1) by intermolecular C–H···π contacts involving the zinc complex molecules and benzene solvate (Table 4). On the other hand, the crystal structure of **4** consists of the mutual parallel shift of neighboring π–stacked 1D strands arranged towards each other (in direction of the arrows given in Fig. 8), owing to the absence of the solvent. This allows the generation of infinite π–stacked pillars perpendicular to the direction of the strand and, in addition, the formation of close π–π contacts between the 3-MePy rings, giving a more compact 2D arrangement. This arrangement is also reflected in the crystal structure of compound **6** (Fig. 9a) but in this case the infinite π–stacking is interrupted due to the significant torsion of the aryldiazenyl-fragment from planarity. The deviation from planarity can be attributed to O_w–H···N and O_w–H···O hydrogen bonding interactions shown in Fig. 9b (see also Table 4) that interconnect the 2D layers in the third dimension. On the contrary, in **2a** and **4** there are no further contacts in the third dimension, but only C–H···O, C–H···N or van der Waals contacts.

In contrast to **2a**, **4** and **6**, in the crystal structure of compound **5a** the L^{XAQ} ligands are not involved in π–interactions and π–π contacts are only found between the 4-MePy ligands and uncoordinated 4-MePy molecules, giving a finite π–stacked assembly formed between four zinc(II) complex molecules and one guest solvate.

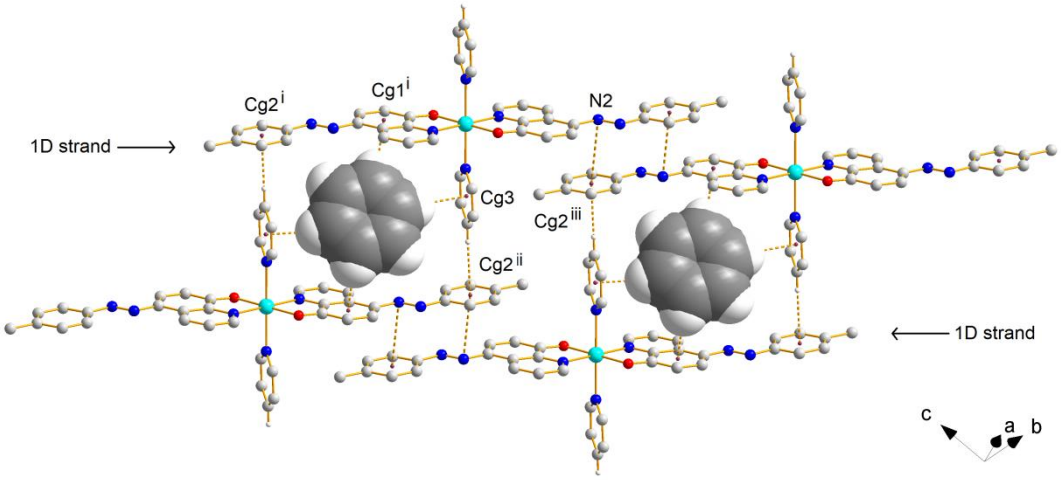

Fig. 8. Fragment of the crystal structure of $[Zn(L^{MeAQ})_2(Py)_2]\cdot C_6H_6$ (**2a**), showing the 2D layers formed through π–π and C–H···π interactions. Cg1 = centroid (C4–C9); Cg2 = centroid (C10–C15); Cg3 = centroid (N4, C17–C21). Symmetry operators: (i) 1-x, -y, 2-z; (ii) -1+x, -1+y, z; (iii) 1-x, 1-y, 1-z. For clarity, hydrogen atoms not involved in hydrogen bonding interactions, and the disorder of the benzene solvate molecule are not shown.

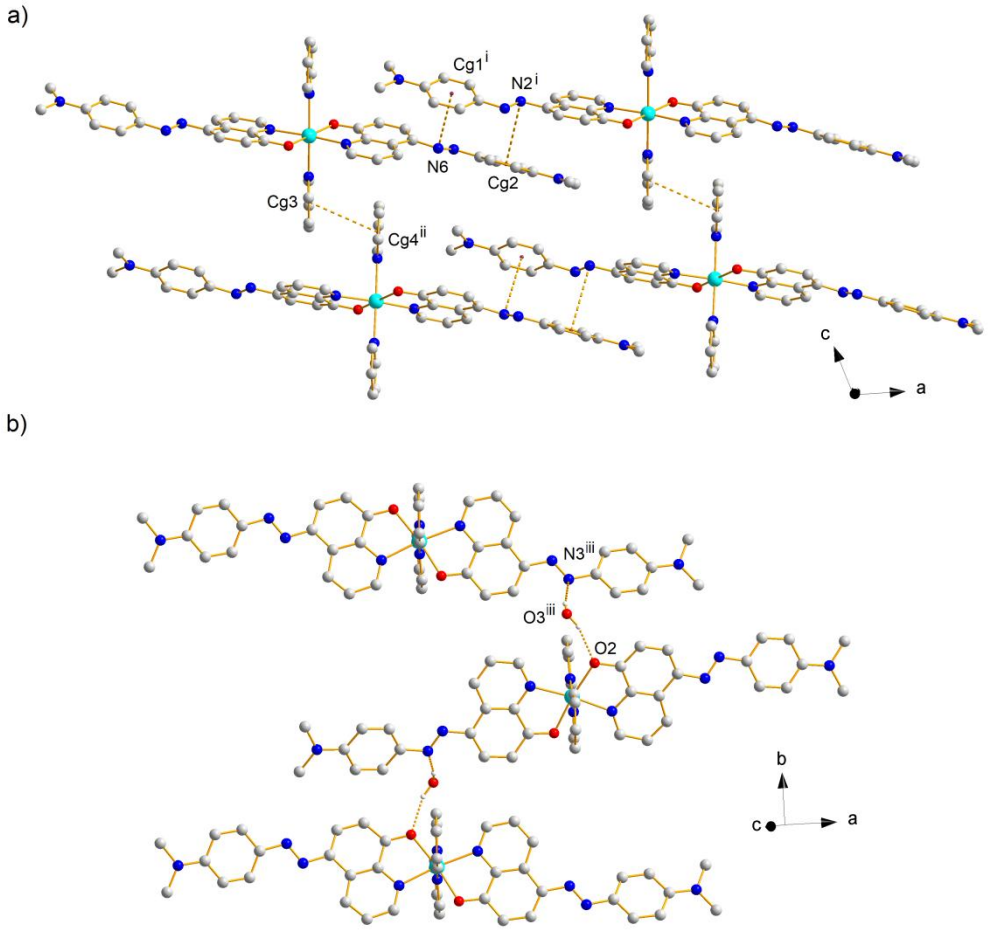

Fig. 9. Fragments of the crystal structure of $[Zn(L^{NMe2AQ})_2(Py)_2]\cdot 1.5C_6H_6\cdot H_2O$ (**6**) showing (a) the 2D layers formed through π–π interactions, and (b) the interconnectivity in the third dimension generated by O_w–H···N and O_w–H···O hydrogen bonds. Cg1 = centroid (C10–C15); Cg2 = centroid (C27–C32); Cg3 = centroid (N9, C35–C39); Cg4 = centroid (N10, C40–C44). Symmetry operators: (i) 1+x, y, z; (ii) x, 1.5-y, -0.5+z; (iii) 1-x, 0.5+y, 1.5-z. For clarity, hydrogen atoms not involved in hydrogen bonding interactions, and benzene solvate molecules are not shown.

*Group II (**2b**, **3**, and **5b**)*

Metal-coordinated water molecules are excellent hydrogen bond donors and it is, therefore, not surprising that the supramolecular interaction patterns for the members of this group are

dominated by hydrogen bonds resulting from the Zn–OH_2 substituents. Although the –C_6H_4–X moieties for **2b**, **3**, and **5b** are different (**2b**, X = Me; **3**, X = OMe; **5b**, X = OEt), the dominant supramolecular aggregation pattern is practically identical. As illustrated in Fig. 10 for compound **2b**, in first instance O_w–H···O_{quin} hydrogen bonding interactions give rise to a staircase-type 1D strand, which is strengthened by π–π contacts involving the 8-quinolinyl groups. The centroid···centroid distances of 3.76 Å shown in Fig. 10a are formed between the different types of aromatic rings in the quinolin-8-olate group, giving relatively short interplanar distances of 3.43 Å. Neighboring 1D strands are linked by additional hydrogen bonds of the O_w–H···O_{quin} type, generating overall 2D hydrogen bonded layers parallel to the *ab* plane (Fig. 10b, Table 4). In the third dimension, the structure is organized essentially by van der Waals contacts. As already mentioned, compounds **3** and **5b** form closely related aggregates with similar hydrogen bonding geometries (Table 4) and identical centroid···centroid and interplanar distances. The main difference is that the 2D layers are parallel to the *bc* plane in these structures.

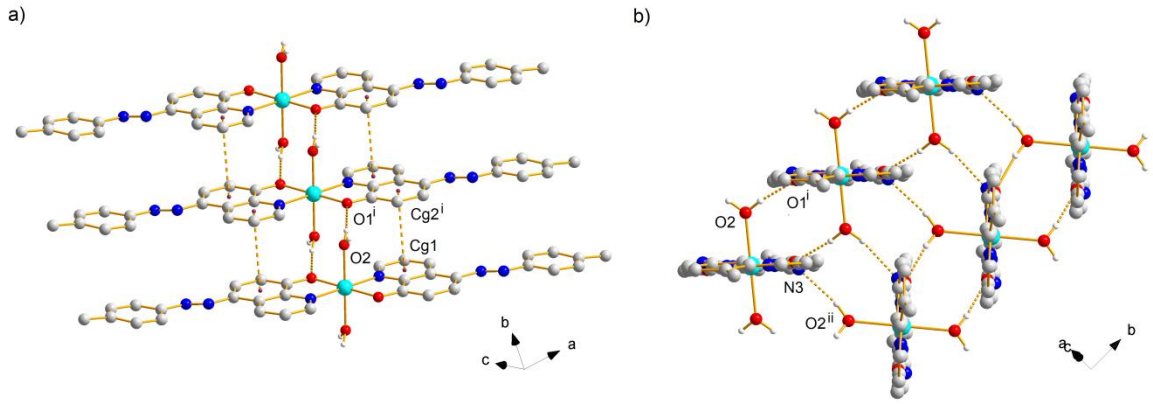

Fig. 10. Fragments of the crystal structure of [Zn(L^{MeAQ})$_2$(H_2O)$_2$] (**2b**) showing (a) the staircase-type π–stacked 1D strands, and (b) their interconnection by O_w–H···O_{quin} hydrogen bonds. Cg1 = centroid (N1, C1–C4, C9); Cg2 = centroid (C4–C9). Symmetry operators: (i) 1.5-x, 2.5-y, 0.5-z; (ii) -0.5+x, 2-y, z. For clarity, hydrogen atoms not involved in hydrogen bonding interactions are omitted.

*Group III (**7** and **8**)*

The halogen-substituted derivatives **7** and **8** are isostructural and comprise V-shaped molecular structures where in first instance the molecules are arranged into 1D strands along *b* through bifurcated C_{py}–H···N_{quin} contacts (Table 4). Neighboring strands are running in opposite directions enabling π–π bonding and the assembly of 2D layers (Fig. 11). In contrast to **2a**, **4** and **6**, the stacking interactions involve now almost the complete π–system of the ligand with interplanar distances of 3.86 and 3.84 Å for **7** and **8**, respectively. Interestingly, in the bromo-derivative **8**, the bromine atoms are involved in Br–π contacts of 3.90 Å (Br···centroid) with the nearby pyridine rings, while the corresponding Cl···centroid distance in compound **7** is 3.99 Å. In the third dimension, the layers are interconnected further only by C–H···π and van der Waals contacts.

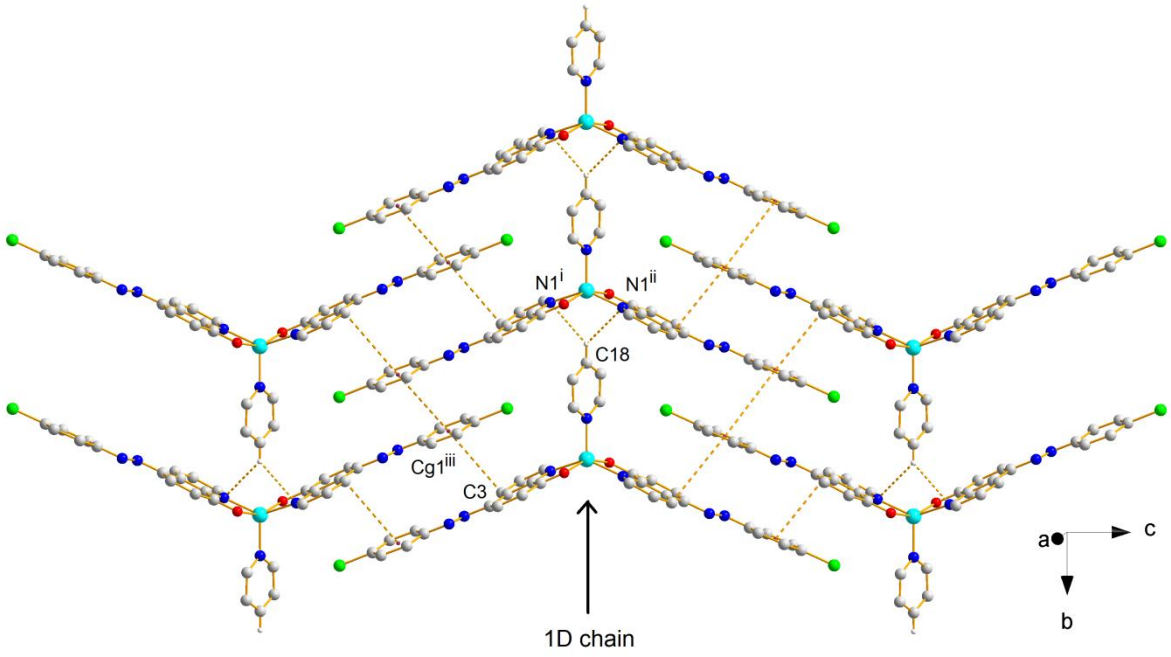

Fig. 11. Fragment of the crystal structure of $[Zn(L^{CAQ})_2(Py)_2]$ (**7**) showing the 2D layers resulting from π–stacking interactions between 1D strands of the V-shaped complex molecules formed through bifurcated C–H···N hydrogen bonds. Cg1 = centroid (C10A–C15A). Symmetry operators: (i) x, -1+y, z; (ii) 0.5-x, -1+y, 1-z; (iii) 0.5-x, 0.5-y, 0.5-z. For clarity, hydrogen atoms not involved in hydrogen bonding interactions and disorder of the aryldiazenyl fragments are omitted.

3.4. Synthesis and characterization of ZnO nanoparticles (NPs)

As described in the introduction section, Zn(II) compounds bearing monotopic quinolin-8-olate derived ligands (Chart 1, **I-XIII**) are actively being researched, owing to their interesting structural aspects and applications. With the availability of a well-characterized series of distorted octahedral (**1**-**6**) and square-pyramidal (**7** and **8**) zinc(II) compounds, it is possible to make use of these compounds as the zinc source for nano-structured materials. As a representative case, $[Zn(L^{MeAQ})_2(Py)_2]\cdot C_6H_6$ (**2a**, Fig. 2a) was selected as potential zinc precursor. In **2a**, two bidentate LMeAQ and two Py ligands stabilize the coordination polyhedron around the zinc atoms, and this structural basis might influence the characteristics of the resulting nanostructures. Using **2a** as precursor, ZnO NPs could be synthesized by an effective and simple method. A two-step procedure was applied; the first step involved the calcination of **2a** to zinc oxide, which in the second step was dispersed in double-distilled water and treated by ultrasonication, affording ZnO NPs. The product was characterized by Powder XRD (PXRD) analysis and imaging techniques such as SEM and TEM.

In the PXRD pattern, the noticeable reflection (lattice) planes are 100, 002, 101, 102, 110, 103, 200, 112, 201, and 202 corresponding to diffraction angles of 31.88°, 34.16°, 36.12°, 47.34°, 56.62°, 62.99°, 66.34°, 68.01°, 69.08° and 76.89°. The XRD pattern reveals that the nanostructures prepared under the above-stated conditions are pure phases and crystalline in nature (Fig. 12) [62]. The observed peaks are in excellent agreement with hexagonal wurtzite structure (JCPDS card No. 36-1451) [63].

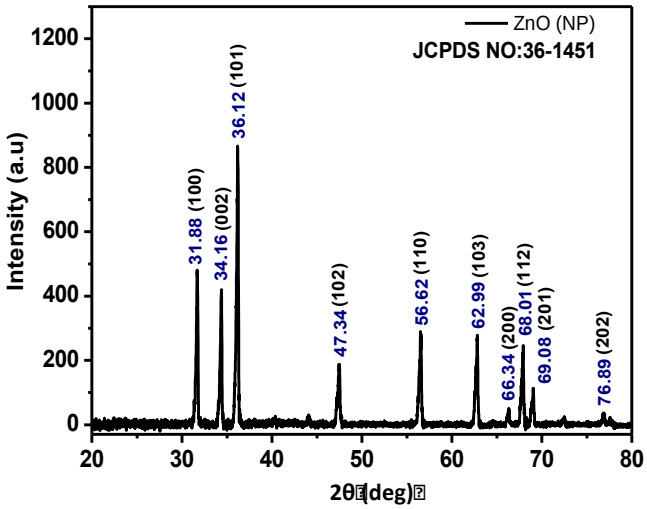

Fig. 12. PXRD pattern of ZnO NPs synthesized from **2a**.

To examine the microstructures of the ZnO NPs, SEM images were recorded (Fig. 13a), revealing a uniform distribution of the ZnO nanostructural morphology. The presence of protrusions and pits between nanoparticles are also distinguishable. The particles are nearly spherical and variable in sizes. Agglomeration of the deposited particles is also evident. The crystalline characteristics and size of the synthesized NPs were determined by TEM. From Fig. 13b, it is observed that the average particle size ranges from 70–120 nm with a slight variation in thickness (for higher magnifications, see Fig. S4, ESI†).

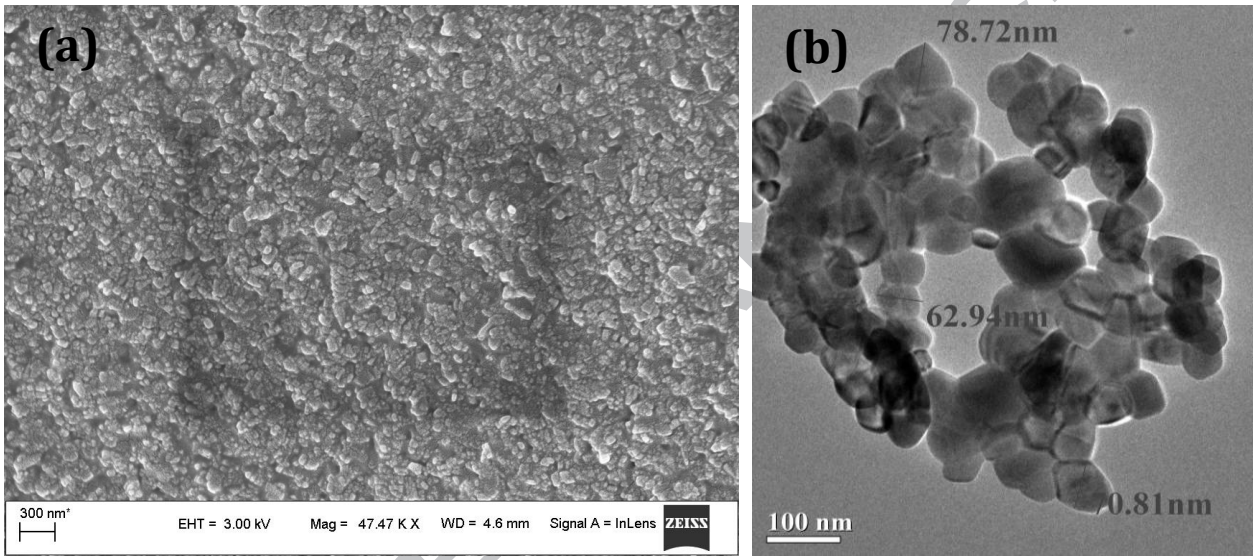

Fig. 13. (a) FE-SEM image and (b) TEM image (magnification 20,000) of ZnO NPs synthesized from **2a**.

3.5. Antibacterial activity results

The solution stability of a drug under physiological conditions is an important pre-requisite for its *in vitro*/ *in vivo* applications and usually, the test compounds are dissolved in dimethylsulfoxide (DMSO) and diluted with test medium prior to *in vitro* testing. Stabilities of the selected zinc(II) compounds 1-8 were assessed in DMSO prior to the antibacterial experiments. The absorbance spectra obtained from UV/Vis were monitored for 2 days (Fig. S5; ESI†); the unchanged basic pattern of the spectra of the test compounds indicated that they are stable in DMSO solution.

The antibacterial potential of the pro-ligands HL^{Q}/ HL^{XAQ} and the corresponding zinc(II)

compounds **1-8** along with $Zn(OAc)_2{\cdot}2H_2O$ was evaluated according to the inhibition zone formation against five indicator bacterial strains, i.e. *Escherichia coli* MTCC 730, *Streptococcus pyogenes* MTCC 1925, *Klebsiella pneumoniae* MTCC 109, *Bacillus cereus* MTCC 430 and *Salmonella enterica* MTCC 735. The results were compared with the activity of chloramphenicol and the solvent used for the experiments (10% DMSO), see Table 5 (Figs. S6 and S7 (Panels A-E); ESI†). As expected, the solvent did not inhibit the growth of the tested microorganisms. Among the eighteen compounds (HL^{Q}/HL^{XAQ} and **1-8)** examined, eleven of them (61%) inhibited at least one of the five indicator organisms, showing different degrees of antimicrobial activity. The results show that the antimicrobial action varies depending on the microorganism and the type of pro-ligand and zinc compound. In general, the Zn compounds exhibited the same or lower activity than the respective pro-ligand and positive control. HL^{Q} gave better antimicrobial activity than the 5-[(4-(X)-phenyl)-1-diazenyl]quinolin-8-ol ligands (HL^{XAQ}) against the bacterial strains used, giving the largest zone of inhibition (25 mm) against *K. pneumoniae*. For the remaining organisms, the inhibitory effect was comparable to the effect of chloramphenicol (Table 4). A comparable activity to that of the standard was observed only for HL^{MeAQ}, when tested against *E. coli* MTCC 730, *S. pyogenes* MTCC 1925, *K. pneumoniae* MTCC 109 and *B. cereus* MTCC 430. HL^{OMeAQ} (except for *S. enterica* MTCC 735), L^{EtAQ} and HL^{OEtAQ} with *p*-OMe, *p*-Et and *p*-OEt substituents were inactive. The most sensitive species was *B. cereus* MTCC 430, on which most of the pro-ligands and their respective zinc(II) compounds acted. On the other hand, the least sensitive species was *S. enterica* MTCC 735, which responded only to pro-ligands HL^{Q} and HL^{OMeAQ}. Seven compounds did not have inhibitory activity against any of the pathogens investigated. The microbial activities of the investigated compounds can be related to several factors such as the type and number of donor atoms and their relative positions within the ligand [30]. Recently, first-row transition metal compounds of 5-chloro-quinolin-8-olate were tested against various species of pathogenic bacteria, clinical isolates and probiotic bacteria. The results indicated that the most sensitive species was *E. faecalis* ATCC 29212 and that the zinc, cobalt and nickel compounds performed better activity than the positive control and the pro-ligand [32].

4. Conclusion

A series new Zn(II) compounds (**1**-**8**) based on HL^{Q} and HL^{XAQ} have been synthesized. Compounds were characterized by spectroscopies while structural information on the molecular and crystal structures was obtained by single-crystal X-ray crystallographic analysis. The results provided three variants of the Zn(II) coordination environment, i.e. $[Zn(L^{XAQ})_2(Py/3\text{-}MePy/4\text{-}MePy)_2]$, $[Zn(L^{XAQ})_2(H_2O)_2]$ and $[Zn(L^{XAQ})_2(Py)]$. The crystal structure analysis evidenced that quinolin-8-olate ligands extended by 4-substituted aryldiazenyl fragments are susceptible to the formation of 1D and 2D π–stacking interactions that are influenced by the metal coordination geometry, the base coordinated to the metal center and the terminal substituent at the ligand. In other words, modification of either of these parameters enables changes in the π–bonding system, which is fundamental for applications in electron conduction and optics. Coordination steered zinc compound **2a** was successfully utilized as precursor for producing nanoparticles. The microbial activities depend on the nature, type and number of donor atoms and their relative positions within the ligand/complex.

Conflict of interest

The authors declare that they have no conflicts of interest with the contents of this article.

Acknowledgments

The financial support of the University Grants Commission, New Delhi (Grant No. 42-396/2013 (SR) 2013, TSBB), the Council of Scientific and Industrial Research, New Delhi (Grant No. 01 (2734)/13/ EMR-II, 2013, TSBB) and the University Grants Commission, New Delhi, India, through SAP-CAS, Phase-I is gratefully acknowledged. KN thanks the University Grants Commission (UGC), New Delhi, for UGC-RGNF research fellowship. Authors (TSBB, KN) acknowledge DST-PURSE for the diffractometer facility.

Supplementary material

CCDC 1811363-1811372 (**1**-**8**) contains the supplementary crystallographic data for this paper. These data can be obtained free of charge from The Cambridge Crystallographic

Data Centre via www.ccdc.cam.ac.uk/data_ request/cif. Supplementary data associated with this article can be found, in the online version, at http:// XXXX. (**Fig. S1** (a) Absorption spectra of pro-ligands HL^{Q} and HL^{XAQ} in DMSO (b) Absorption spectra of zinc(II) compounds **1-8** in DMSO. For the purpose of clarity, the absorption spectra of structurally related compounds are grouped together, viz., (c) compounds **2a** and **2b**, (d) compounds **1**, **2a**, **4**, **5a** and **6**, (e) compounds **5a** and **5b**, (f) compounds **2b**, **3** and **5b**, (g) compounds **7** and **8**. **Fig. S2.** Emission spectra of (**a**) HL^{NMe2AQ} (λ_{ex} = 470 nm) and $[Zn(L^{NMe2AQ})_2(Py)_2]\cdot 1.5C_6H_6\cdot H_2O$ (**6**) (λ_{ex} = 433 nm) in DMSO (**b**) pro-ligands HL^{Q} (λ_{ex} = 317 nm) and $[Zn(L^{Q})_2(4\text{-}MePy)_2]\cdot H_2O$ (**1**) (λ_{ex} = 402 nm) in DMSO solution (solid line) and in solid-state (broken lines). **Fig. S3.** Perspective views of the asymmetric unit of the crystal structures of compounds **1-8**. Ellipsoids are drawn at the 30% probability level. For clarity, uncoordinated solvents in compounds **1**, **2a** and **5a**, and the disorder in compounds **4**, **7** and **8** are not shown. **Fig. S4.** TEM images of ZnO NPs synthesized from **2a** with (a) 40-, (b) 80-, (c) 120- and (d) 500,000-fold magnifications. **Fig. S5.** Uv-Vis absorption spectra over time for Zn(II) compounds **1-8** in DMSO. **Fig. S6.** Graphics showing the zones of inhibition around the wells containing the compounds tested in the present study. For the abbreviations of pro-ligands (HL^{Q}/HL^{XAQ}) and the zinc(II) compounds (**1-8**), refer to Scheme 1. **Fig. S7.** Petri dishes showing the antimicrobial activity of the pro-ligands HL^{Q}/ HL^{XAQ} and the corresponding zinc(II) compounds (**1-8**) (Scheme 1) against five bacterial strains, as determined by the inhibition zone method. Compounds excluded from present studies have been marked with red cross sign. **Table S1.** Visible absorption maxima from the electronic spectra of pro-ligands HL^{Q} and HL^{XAQ} and the Zn(II) compounds **1-8** in DMSO solution.)

References

[1] J. Mendham, R. C. Denny, J. D. Barnes, M. J. K. Thomas, Vogel's Quantitative Chemical Analysis, Prentice Hall, London, 2000.

[2] D. C. Harris, Quantitative Chemical Analysis, Freeman, New York, 2010.

[3] H. Kunkely, A. Vogler, Chem. Phys. Lett. 304 (1999) 187-190.

[4] H. Kunkely, A. Vogler, J. Photochem. Photobiol. A Chem. 144 (2001) 69-72.

[5] H. Kunkely, A. Vogler, Chem. Phys. Lett. 376 (2003) 226-229.

[6] A. Strasser, A. Vogler, Inorg. Chim. Acta 357 (2004) 2345-2348.

[7] H. Kunkely, A. Vogler, Inorg. Chim. Acta 362 (2009) 196-198.

[8] L. S. Sapochak, A. Padmaperuma, N. Washton, F. Endrino, G. T. Schmett, J. Marshall, D. Fogarty, P. E. Burrows, S. R. Forrest, J. Am. Chem. Soc. 123 (2001) 6300-6307.

[9] L. Li, B. Xu, Tetrahydron 64 (2008) 10986-10995.

[10] L. Wang, X. Jiang, Z. Zhang, S. Xu, Displays 21 (2000) 47-49.

[11] C. W. Tang, S. A. Van Slyke, Appl. Phys. Lett. 51 (1987) 913-915.

[12] F. O. Suliman, I. Al-Nafai, S. N. Al-Busafi, Spectrochim. Acta A 118 (2014) 66-72.

[13] M. Albrecht, M. Fiege, O. Osetska, Coord. Chem. Rev. 252 (2008) 812-824.

[14] C-H. Lee, J-H. Jeon, S-G. Lee, H-S. Lee, J. Korean Soc. Appl. Biol. Chem. 53 (2010) 464-469.

[15] C. M. Darby, C. F. Nathan, J. Antimicrob. Chemother. 65 (2010) 1424-1427.

[16] A. Budimir, Acta Pharm. 61 (2011) 1-14.

[17] V. Corce, E. Morin, S. Guiheneuf, E. Renault, S. Renaud, I. Cannie, R. Tripier, L. M. P. Lima, K. Julienne, S. G. Gouin, O. Loreal, D. Deniaud, F. Gaboriau, Bioconjugate Chem. 23 (2012) 1952-1968.

[18] V. Oliveri, M. L. Giuffrida, G. Vecchio, C. Aiello, M. Viale, Dalton Trans. 41 (2012) 4530-4535.

[19] V. Prachayasittikul, S. Prachayasittikul, S. Ruchirawat, V. Prachayasittikul, Drug. Des. Dev. Ther. 7 (2013) 1157-1178.

[20] K. G. Naber, H. Niggemann, G. Stein, G. Stein, BMC Infect. Dis. 14 (2014) 628.

[21] J. Lazovic, L. Guo, J. Nakashima, L. Mirsadraei, W. Yong, H. J. Kim, B. Ellingson, H. Wu, W. B. Pope, Neuro-Oncol. 17 (2015) 53-62.

[22] W. Chan-On, N. T. B. Huyen, N. Songtawee, W. Suwanjang, S. Prachayasittikul, V. Prachayasittikul, Drug Des. Dev. Ther. 9 (2015) 2033-2047.

[23] E. Skrivanova1, F. V. Immerseel, P. Hovorkova, L. Kokoska, PLoS ONE 11 (2016) e0167638.

[24] H.-R. Zhang, Y.-C. Liu, Z.-F. Chen, T. Meng, B.-Q. Zou, Y.-N. Liua, H. Liang, New J. Chem. 40 (2016) 6005-6014.

[25] R. Cherdtrakulkiat, S. Boonpangrak, N. Sinthupoom, S. Prachayasittikul, S. Ruchirawat, V. Prachayasittikul, Biochem. Biophys. Rep. 6 (2016) 135-141.

[26] D. K. Blencowe, A. P. Morby, FEMS Microbiol. Rev. 27 (2003) 291-311.

[27] J. Yao, Y. Liu, H. G. Liang, C. Zhang, J. Z. Zhu, X. Qin, M. Sun, S. S. Qu, Z. N. Yu, J. Therm. Anal. Calorim. 79 (2005) 39-43.

[28] S. Atmaca, K. Gul, R. Cicek, Turk. J. Med. Sci. 28 (1998) 595-597.

[29] Z. Q. Li, F. J. Wu, Y. Gong, C. W. Hu, Y. H. Zhang, M. Y. Gan, Chin. J. Chem. 25 (2007) 1809-1814.

[30] S. H. Auda, I. Knutter, B. Bretschneider, M. Bransch, Y. Mrestani, C. Crobe, R. H. H. Neubert, Pharmaceuticals, 2 (2009) 184-193.

[31] R. G. W. Hollingshead, Oxine and Its Derivatives, vol. III, Butterworths Scientific Publications, London, 1956.

[32] I. Potočňák, P. Vranec, V. Farkasová, D. Sabolová, M. Vataščinová, J. Kudláčová, I. D. Radojević, L. R. Čomić, B. S. Markovic, V. Volarevic, N. Arsenijevic, S. R. Trifunović, J. Inorg. Biochem. 154 (2016) 67-77.

[33] M. Albrecht, O. Blau, R. Fröhlich, Chem. Eur. J. 5 (1999) 48-56.

[34] L. L. Merritt, R. T. Cady, B. W. Mundy, Acta Crystallogr. 7 (1954) 473-476.

[35] Y.-M. Hu, J. Qu, Y.-L. Yi, H.-L. Gao, J.-Z. Cui, J. Coord. Chem. 66 (2013) 18-27.

[36] Y. Kai, M. Morita, N. Yasuoka, N. Kasai, Bull. Chem. Soc. Jpn. 58 (1985) 1631-1635.

[37] L. S. Sapochak, F. E. Benincasa, R. S. Schofield, J. L. Baker, K. K. C. Ricco, D. Fogarty, H. Kohlmann, K. F. Ferris, P. E. Burrows, J. Am. Chem. Soc. 124 (2002) 6119-6125.

[38] a) M. Czugler, R. Neumann, E. Weber, Inorg. Chim. Acta 313 (2001) 100-108. b) G. Z. Yuan, Y. P. Huo, X. L. Nie, X. M. Fang, S. Z. Zhu, Tetrahedron 68 (2012) 8018-8023.

[39] J. Zhang, R. G. Xiong, Z. F. Chen, X. Z. You, G. H. Lee, S. M. Peng, Chem. Lett. 30 (2001) 676-677.

[40] M. Albrecht, K. Witt, P. Weis, E. Wegelius, R. Fröhlich, Inorg. Chim. Acta 341 (2002) 25-32.

[41] P. Khakhlary, J. B. Baruah, J. Chem. Sci. 127 (2015) 215-223.

[42] a) T. Li, J. Yang, X. J. Hong, Y. J. Ou, Z. G. Gu, Y. P. Cai, CrystEngComm. 16 (2014) 3848-3852. b) T. Li, X. J. Hong, X. Liu, R. Chen, Q. G. Zhan, X. Xu, Y. P. Cai, CrystEngComm. 16 (2014) 3883-3889. c) Z. G. Gu, Y. T. Liu, X. J. Hong, Q. G. Zhan, Z. P. Zheng, S. R. Zheng, W. S. Li, S. J. Hu, Y. P. Cai, Cryst. Growth Des. 12 (2012) 2178-2186. d) Y. Gai, F. Jiang, L. Chen, M. Wu, K. Su, J. Pan, X. Wan, M. Hong, Cryst. Growth Des. 14 (2014) 1010-1017.

[43] a) M. D. Zhang, L. Qin, H. T. Yang, Y. Z. Li, Z. J. Guo, H. G. Zheng, Cryst. Growth Des. 13 (2013) 1961-1969. b) X. X. Zhou, H. C. Fang, Y. Y. Ge, Z. Y. Zhou, Z. G. Gu, X. Gong, G. Zhao, Q. G. Zhan, R. H. Zeng, Y. P. Cai, Cryst. Growth Des. 10 (2010) 4014-4022.

[44] a) G. Z. Yuan, Y. P. Huo, X. L. Nie, H. Jiang, B. Liu, X. M. Fang, F. H. Zhao, Dalton Trans. 42 (2013) 2921-2929. b) G. Z. Yuan, L. L. Rong, X. L. Qiao, L. Ma, X. W. Wei, CrystEngComm. 15 (2013) 7307-7314. c) G. Z. Yuan, W. L. Shan, X. L. Qiao, L. Ma, Y. P. Huo, Chem. – Asian J. 9 (2014) 1913-1921. d) G. Z. Yuan, W. L. Shan, B. Liu, L. L. Rong, L. Y. Zhang, H. Zhang, X. W. Wei, Dalton Trans. 43 (2014) 9777-9785. e) L. Y. Zhang, L. L. Rong, G. L. Hu, S. Jin, W.-G. Jia, J. Liu, G. Z. Yuan, Dalton Trans. 44 (2015) 6731-6739. f) L. Y. Zhang, L. Y. Sun, X. Y. Li, Y. L. Tian, G. Z. Yuan, Dalton Trans. 44 (2015) 401-410. g) W.-B. Yu, Q.-Y. He, H.-T. Shi, G. Z. Yuan, X. W. Wei, Chem. – Asian J. 10 (2015) 239-246. h) G. Yuan, G. Hu, W. Shan, S. Jin, Q. Gu, J. Chen, Dalton Trans. 44 (2015) 17774-17783.

[45] a) N. Donze, P. Pechy, M. Gratzel, M. Schaer, L. Zuppiroli, Chem. Phys. Lett. 315 (1999) 405-410. b) Q. L. Huang, J. F. Li, T. J. Marks, J. Appl. Phys. 101 (2007) 093101. c) K. Sokołowski, I. Justyniak, W. Śliwiński, K. Sołtys, A. Tulewicz, A. Kornowicz, R. Moszyński, J. Lipkowski, J. Lewiński, Chem. Eur. J. 18 (2012) 5637-5645.

[46] A. Vogler, Inorg. Chem. Commun. 45 (2014) 82-83.

[47] S. Takamoto, Q. Fernando, H. Freiser, Anal. Chem. 37 (1965) 1249-1251.

[48] V. M. Ivanov, T.F. Rudometkina, Zh. Anal. Khim. 33 (1978) 2426.

[49] a) T. S. Basu Baul, A. Mizar, X. Song, G. Eng, R. Jirásko, M. Holčapek, R. Willem, M. Biesemans, I. Verbrugge, R. Butcher, J. Organomet. Chem. 691 (2006) 2605-2613. b) T.S. Basu Baul, A. Mizar, A. Lyčka, E. Rivarola, R. Jirásko, M. Holčapek, D. de Vos, U. Englert, J. Organomet. Chem. 691 (2006) 3416-3425. c) T. S. Basu Baul, A. Mizar, E. Rivarola, U. Englert,

J. Organomet. Chem. 693 (2008) 1751-1758. d) T. S. Basu Baul, A. Mizar, A. K. Chandra, X. Song, G. Eng, R. Jirásko, M. Holčapek, D. de Vos, A. Linden, J. Inorg. Biochem. 102 (2008) 1719-1730. e) T. S. Basu Baul, A. Mizar, A. Paul, G. Ruisi, R. Willem, M. Biesemans, A. Linden, J. Organomet. Chem. 694 (2009) 2142-2152.

[50] M. Hebrant, M. Rose-Helene, J.-P. Joly, A. Walcarius, Colloids Surf. A, Physicochem. Eng. Aspects 380 (2011) 261-269.

[51] R. Sarkar, P. Mondal, K. K. Rajak, Dalton Trans. 43 (2014) 2859-2877.

[52] M. Ghedini, M. La Deda, I. Aiello, A. Grisolia, J. Chem. Soc., Dalton Trans. (2002) 3406-3409.

[53] M. La Deda, A. Grisolia, I. Aiello, A. Crispini, M. Ghedini, S. Belviso, M. Amati, F. Lelj, J. Chem. Soc., Dalton Trans. (2004) 2424-2431.

[54] A. Z. El-Sonbati, R. M. Issa, A. M. Abd El-Gawad, Spectrochim. Acta, Part A 68 (2007) 134-138.

[55] a) T. S. Basu Baul, S. Kundu, S. Mitra, H. Höpfl, E. R. T. Tiekink, A. Linden, Dalton Trans. 42 (2013)1905-1920. b) T. S. Basu Baul, S. Kundu, H. Höpfl, E. R. T. Tiekink, A. Linden, Polyhedron 55 (2013) 270-282. c) T. S. Basu Baul, S. Kundu, S. W. Ng, E. R. T. Tiekink, Acta Crystallogr. E69 (2013) m623-m624. d) T. S. Basu Baul, S. Kundu, A. Linden, N. Raviprakash, S. Manna, F. Guedes da Silva, Dalton Trans. 43 (2014) 1191-1202. e) T. S. Basu Baul, S. Kundu, S. W. Ng, N. Guchhait, E. R. T. Tiekink, J. Coord. Chem. 67 (2014) 96-119. f) T. S. Basu Baul, S. Kundu, H. Höpfl, E. R. T. Tiekink, A. Linden, J. Coord. Chem. 67 (2014) 1061-1078. g) T. S. Basu Baul, S. Kundu, P. Singh, Shaveta, F. Guedes da Silva, Dalton Trans. 44 (2015) 2359-2369.

[56] Agilent Technologies. CrysAlisPro, Version 1.171.37.35. Yarnton, Oxfordshire, United Kingdom: 2014.

[57] O. V. Dolomanov, L. J. Bourhis, R. J. Gildea, J. A. K. Howard and H. Puschmann, J. Appl. Cryst. 42 (2009) 339-341.

[58] a) G. M. Sheldrick, Acta Crystallogr., Sect. A: Found Adv. 71 (2015) 3-8. b) G. M. Sheldrick, Acta Crystallogr., Sect. C: Struct. Chem. 71 (2015) 3-8.

[59] K. Brandenburg, Diamond, Version 4.3.2, Crystal Impact GbR, Bonn, Germany, 2017.

[60] C. Perez, M. Paul, P. Bazerque, Acta Bio. Med. Exp. 15 (1990) 113-115.

[61] F. H. Allen, Acta Crystallogr. B 258 (2000) 380-388.

[62] J. L. G. Fierroi, Metal Oxides: Chemistry & Applications. CRC Press. p. 182, 2006.

[63] K. A. Alim, V. A. Fonoberov, M. Shamsa, A. A. Balandin, J. Appl. Phys. 97 (2005) 124313.

Table 1

Crystal data, data collection parameters and convergence results for compounds **1-8**

	1	**2a**	**2b**	**3**	**4**	**5a**	**5b**	**6**	**7**	**8**
CCDC No.	1811363	1811364	1811365	1811368	1811366	1811372	1811367	1811371	1811369	1811370
Empirical formula	$C_{30}H_{26}N_4O_2Zn$, H_2O	$C_{42}H_{34}N_8O_2Zn$, C_6H_6	$C_{32}H_{28}N_6O_4Zn$	$C_{32}H_{28}N_6O_6Zn$	$C_{46}H_{42}N_8O_2Zn$	$2(C_{46}H_{42}N_8O_4Zn)$, C_6H_7N	$C_{34}H_{32}N_6O_6Zn$	$C_{44}H_{40}N_{10}O_2Zn$, $1.5(C_6H_6)$, H_2O	$C_{35}H_{23}Cl_2N_7O_2Zn$	$C_{35}H_{23}Br_2N_7O_2Zn$
Formula weight	557.93	826.25	625.97	657.97	804.24	1765.61	686.02	941.41	709.87	798.79
Temperature (K)	295.2(8)	290.74(10)	292.5(4)	293.6(6)	291.08(12)	296.0(10)	292.46(10)	293(2)	291.6(3)	291.72(10)
Crystal system	tetragonal	triclinic	monoclinic	monoclinic	triclinic	triclinic	monoclinic	monoclinic	monoclinic	monoclinic
Space group	$P4_322$	P-1	$I2/a$	$P2_1/c$	P-1	P-1	$P2_1/c$	$P2_1/c$	$I2/a$	$C2/c$
a (Å)	13.6993(5)	8.3838(5)	18.6752(11)	16.0255(6)	9.5838(10)	11.7094(10)	17.6548(11)	17.2611(11)	12.2341(16)	32.1654(11)
b (Å)	13.6993(5)	10.9391(8)	5.1678(3)	5.22408(18)	10.4815(11)	14.6298(12)	5.2005(3)	15.9628(9)	8.3020(9)	8.2676(4)
c (Å)	14.3499(7)	11.4089(6)	31.2749(14)	18.4660(8)	11.9203(15)	14.8110(11)	18.5132(11)	18.1535(11)	31.802(4)	12.4211(5)
α (°)	90	98.682(5)	90	90	65.794(11)	65.469(8)	90	90	90	90
β (°)	90	90.709(4)	106.487(5)	108.907(4)	70.625(10)	72.127(7)	110.052(7)	108.144(6)	100.898(10)	101.133(3)
y (°)	90	95.627(5)	90	90	76.097(9)	88.046(7)	90	90	90	90
Volume (Å^3)	2693.1(2)	1028.95(11)	2894.2(3)	1462.54(10)	1022.7(2)	2184.0(3)	1596.75(18)	4753.2(5)	3171.8(7)	3241.0(2)
Z	4	1	4	2	1	1	2	4	4	4
ρ_{calc} (g/cm^3)	1.376	1.333	1.437	1.494	1.306	1.342	1.427	1.316	1.487	1.637
μ (mm^{-1})	0.950	0.647	0.897	0.897	0.649	0.618	0.825	0.572	0.988	3.268
F(000)	1160.0	430.0	1296.0	680.0	420.0	922.0	712.0	1972.0	1448.0	1592.0
Crystal size (mm^3)	0.24 × 0.21 × 0.21	0.28 × 0.23 × 0.11	0.15 × 0.13 × 0.13	0.30 × 0.15 × 0.05	0.56 × 0.23 × 0.23	0.25 × 0.25 × 0.21	0.30 × 0.20 × 0.15	0.21 × 0.17 × 0.11	0.07 × 0.05 × 0.05	0.56 × 0.09 × 0.03
2Θ range for data collection (°)	6.41-52.74	6.00-57.54	8.00-57.37	5.86-57.52	6.62-57.70	6.16-57.32	7.25-57.26	6.44-50.00	6.25-57.70	5.95- 57.48
Index ranges	-17 ≤ h ≤ 17 -15 ≤ k ≤ 15 -17 ≤ l ≤ 10	-11 ≤ h ≤ 10 -11 ≤ k ≤ 14 -14 ≤ l ≤ 14	-22 ≤ h ≤ 23 -6 ≤ k ≤ 6 -41 ≤ l ≤ 41	-19 ≤ h ≤ 21 -6 ≤ k ≤ 6 -24 ≤ l ≤ 24	-10 ≤ h ≤ 12 -13 ≤ k ≤ 13 -16 ≤ l ≤ 16	-15 ≤ h ≤ 14 -19 ≤ k ≤ 19 -18 ≤ l ≤ 19	-23 ≤ h ≤ 23 -6 ≤ k ≤ 4 -23 ≤ l ≤ 24	-18 ≤ h ≤ 20 -18 ≤ k ≤ 16 -21 ≤ l ≤ 21	-15 ≤ h ≤ 15 -8 ≤ k ≤ 11 -41 ≤ l ≤ 40	-42 ≤ h ≤ 42 -11 ≤ k ≤ 11 -16 ≤ l ≤ 16
Reflections collected	6424	8038	6331	6506	7792	17184	6575	20008	13650	15226
Independent reflections [R_{int}]	2762 [0.026]	4646 [0.022]	3303 [0.037]	3359 [0.033]	4653 [0.017]	9853 [0.037]	3619 [0.026]	8342 [0.050]	3790 [0.096]	3875 [0.055]
Data/restraints/parameters	2762/0/177	4646/72/284	3303/2/203	3359/2/212	4653/444/355	9853/0/588	3619/2/221	8342/86/617	3790/210/254	3875/180/254
Goodness-of-fit on F^2	1.060	1.049	1.027	1.048	1.052	1.045	1.046	1.060	0.975	1.029
R_1 [$I \geq 2\sigma(I)$]	0.0314	0.0455	0.0500	0.0423	0.0501	0.0602	0.0400	0.0613	0.0638	0.0518
wR_2 [all data]	0.0718	0.1220	0.1187	0.0897	0.1420	0.1316	0.0896	0.1480	0.1548	0.1059
Largest diff. peak/hole (e Å^{-3})	0.15/-0.17	0.48/-0.37	0.42/-0.39	0.28/-0.30	0.68/-0.62	0.35/-0.33	0.28/-0.39	0.60/-0.40	0.32/-0.47	0.52/-0.36
Flack parameter	0.016(9)	-	-	-	-	-	-	-	-	-

Table 2

Selected bond lengths (Å) and intramolecular distances (Å) for compounds **1**-**8**.[a]

	1	**2a**	**2b**	**3**	**4**[b]	**5a** (A)[c]	**5a** (B)[c]	**5b**	**6**	**7**	**8**
$Zn–O_{quin}$	2.0684(19)	2.0635(15)	2.0604(19)	2.0620(15)	2.0478(16)	2.0535(19)	2.063(2)	2.0669(14)	2.058(2) 2.070(2)	2.043(3)	2.039(2)
$Zn–N_{quin}$	2.134(2)	2.0985(18)	2.152(2)	2.1159(8)	2.1052(19)	2.104(2)	2.114(3)	2.1196(17)	2.141(3) 2.109(3)	2.092(3)	2.102(3)
$Zn–N_{py}$	2.273(4) 2.217(4)	2.2785(19)	-	-	2.200(5)	2.248(3)	2.244(2)	-	2.258(3) 2.263(3)	2.013(5)	2.035(4)
$Zn–O_w$	-	-	2.175(2)	2.1781(17)	-	-	-	2.1794(17)	-	-	-

[a] Except for **6**, the molecular structures of all compounds exhibit crystallographic symmetry (2-axis for **1**, **7** and **8**; inversion symmetry for **2a**, **2b**, **3**, **4**, **5a**, and **5b**).

[b] The molecular structure exhibits disorder of the 3-methylpyridine ligand. Distances are only given for the most abundant constitution.

[c] The asymmetric unit contains two crystallographically independent molecule halves and are labeled A and B.

Table 3

Selected bond angles (°) for compounds **1**-**8**.[a]

	1	**2a**	**2b**	**3**	**4**[b]	**5a** (A)[c]	**5a** (B)[c]	**5b**	**6**	**7**	**8**
O_{quin}–Zn–N_{quin} (chelate)	80.32(9)	81.11(6)	80.37(8)	80.45(6)	81.19(7)	80.91(8)	80.85(9)	80.48(6)	80.27(10) 80.52(11)	79.41(12)	79.99(10)
O_{quin}–Zn–N_{quin} (interligand)	99.62(9)	98.89(6)	99.63(8)	99.55(6)	98.81(7)	99.09(8)	99.15(9)	99.52(6)	93.33(11) 105.93(11)	92.53(13)	92.37(10)
O_{quin}–Zn–O_{quin}	172.81(14)	180.0	180.0	180.0	180.0	180.0	180.0	180.0	172.93(9)	156.33(17)	156.86(16)
N_{quin}–Zn–N_{quin}	179.11(16)	180.0	180.0	180.0	180.0	180.0	180.0	180.0	173.49(12)	140.21(18)	141.42(17)
N_{py}–Zn–N_{py}	180.0	180.0	-	-	180.0	180.0	180.0	-	175.95(12)	-	-
N_{py}–Zn–O_{quin}	86.41(7) 93.59(7)	89.12(6) 90.88(6)	-	-	91.9(2) 88.1(2)	92.40(9) 87.60(9)	91.45(9) 88.55(9)	-	88.62(11) 88.52(11) 94.87(11) 88.28(11)	101.84(9)	101.57(8)
N_{py}–Zn–N_{quin}	89.55(8) 90.45(8)	89.08(7) 90.92(7)	-	-	88.8(2) 91.2(2)	90.84(9) 89.16(9)	90.64(9) 89.36(9)	-	89.75(11) 88.28(11) 89.60(11) 92.76(11)	109.89(9)	109.29(8)
O_w–Zn–O_w	-	-	180.0	180.0	-	-	-	180.0	-	-	-
O_w–Zn–O_{quin}	-	-	90.79(8) 89.21(8)	90.08(7) 89.92(7)	-	-	-	90.21(6) 89.79(6)	-	-	-
O_w–Zn–N_{quin}	-	-	89.72(9) 90.27(9)	89.80(7) 90.20(7)	-	-	-	90.07(6) 89.93(6)	-	-	-

[a] Except for **6**, the molecular structures of all compounds exhibit crystallographic symmetry (2-axis for **1**, **7** and **8**; inversion symmetry for **2a**, **2b**, **3**, **4**, **5a**, and **5b**).

[b] The molecular structure exhibits disorder of the 3-methylpyridine ligand. Distances are only given for the most abundant constitution.

[c] The asymmetric unit contains two crystallographically independent molecule halves and are labeled A and B.

Table 4

Geometric parameters for the hydrogen bonding interactions in the crystal structures of **2-8**.

Compound	Intermolecular interaction	D–H/[Å]	D···A/[Å]	H···A/[Å]	∠DHA/[°]	Symmetry code
Group I						
2a	C19–H19···Cg2	0.93	3.681	2.75	176	-1+x, -1+y, z
6	O3–H3A···N3	0.85	3.035(5)	2.19	170	x, y, z
	O3–H3B···O2	0.85	2.800(4)	1.99	160	1-x, -0.5+y, 1.5-z
Group II						
2b	O2–H2A···N3	0.85	2.948(3)	2.12	165	0.5+x, 2-y, z
	O2–H2B···O1	0.85	2.666(3)	1.83	171	1.5-x, 2.5-y, 0.5-z
3	O2–H2A···N3	0.85	2.933(2)	2.13	158	1-x, 0.5+y, 1.5-z
	O2–H2B···O1	0.85	2.680(2)	1.83	173	x, 1+y, z
5b	O3–H3A···N3	0.85	2.934(2)	2.11	163	2-x, -0.5+y, 1.5-z
	O3–H3B···O1	0.85	2.675(2)	1.84	168	x, -1+y, z
Group III						
7	C18–H18···N1	0.93	3.462(9)	2.75	134	x, -1+y, -z
	C18–H18···N1	0.93	3.462(9)	2.75	134	0.5-x, -1+y, 1-z
8	O1–H1'···O6	0.93	3.446(7)	2.74	134	x, 1+y, z
	C5–H5···O1	0.93	3.446(7)	2.74	134	1-x, 1+y, 1.5-z

Table 5

Antimicrobial activity of ligands HL^{Q}/HL^{XAQ} and the corresponding zinc(II) compounds (**1**-**8**) against five bacterial strains.

Pro-ligand/ Compound	Inhibition zones (in mm) observed for the tested bacterial species				
	E. coli MTCC 730	*S. pyogenes* MTCC 1925	*K. pneumoniae* MTCC 109	*B. cereus* MTCC 430	*S. enterica* MTCC 735
HL^{Q}	17	22	25	20	16
1	-	10	-	10	-
HL^{MeAQ}	13	12	13	13	-
2a	10	-	10	-	-
2b	10	-	10	10	-
HL^{OMeAQ}	-	-	-	-	10
3	-	-	-	-	-
HL^{EtAQ}	-	-	-	-	-
4	-	10	10	10	-
HL^{OEtAQ}	-	-	-	-	-
5a	-	-	-	-	-
5b	-	-	-	-	-
HL^{NMe2AQ}	-	-	10	10	-
6	-	-	-	-	-
HL^{CAQ}	-	-	10	13	-
7	-	-	-	-	-
HL^{BAQ}	-	-	-	10	-
8	-	-	-	10	-
$Zn(OAc)_2 \cdot 2H_2O$	-	-	-	-	-
Solvent (10% DMSO)	-	-	-	-	-
Chloramphenicol	25	25	25	25	25

Highlights

- Ten new Pyridine assisted bis(quinolin-8-olato)zinc(II) compounds with distorted octahedral and square-pyramidal geometries have been synthesized.
- Structural characterizations of the compounds were accomplished from IR, ^{1}H, ^{13}C, Uv-Vis and fluoroscence spectroscopy.
- All the compounds have been characterized by single crystal X-ray crystallography.
- Applications of the compounds toward the formation of nanomaterials and antibacterial activity are reported.

[PICTOGRAM FOR GRAPHICAL ABSTRACT]

Pyridine aided progression from amorphous to crystalline bis([5-(aryl)-1-diazenyl]quinolin-8-olato) zinc(II) compounds – Solution and solid-state structural characterization, nanoparticle formation and antibacterial activity

Tushar S. Basu Baul,[a,*] Khrawborlang Nongsiej,[a] Koel Biswas,[b] Santa Ram Joshi[b] and Herbert Höpfl[c,*]

Pyridine assisted bis(quinolin-8-olato)zinc(II) compounds with distorted octahedral and square-pyramidal geometries were synthesized and their applications are reported.